

**MATHEMATICAL ENGINEERING
TECHNICAL REPORTS**

**Distributed Formation Control for
Target-enclosing Operation
by Multiple Dynamic Agents
based on a Cyclic Pursuit Strategy**

Shinji HARA, Tae-Hyoung KIM and Yutaka HORI

(Communicated by Kazuo MUROTA)

METR 2007-62

December 2007

DEPARTMENT OF MATHEMATICAL INFORMATICS
GRADUATE SCHOOL OF INFORMATION SCIENCE AND TECHNOLOGY
THE UNIVERSITY OF TOKYO
BUNKYO-KU, TOKYO 113-8656, JAPAN

WWW page: <http://www.keisu.t.u-tokyo.ac.jp/research/techrep/index.html>

The METR technical reports are published as a means to ensure timely dissemination of scholarly and technical work on a non-commercial basis. Copyright and all rights therein are maintained by the authors or by other copyright holders, notwithstanding that they have offered their works here electronically. It is understood that all persons copying this information will adhere to the terms and constraints invoked by each author's copyright. These works may not be reposted without the explicit permission of the copyright holder.

Distributed Formation Control for Target-enclosing Operation by Multiple Dynamic Agents based on a Cyclic Pursuit Strategy

Shinji HARA*, Tae-Hyoung KIM†, Yutaka HORI‡

December 26th, 2007

Abstract

This paper studies a design methodology of a distributed cooperative controller for target-enclosing operations by multiple dynamic agents. To this end, we first present an on-line path generator design method based on a cyclic pursuit scheme. Then, we provide the stability condition which the developed path generator should satisfy. This condition is derived based on a simple stability analysis method for hierarchical large-scale linear systems with generalized frequency variable. The formation control scheme combined with a cyclic pursuit based distributed on-line path generator satisfying the derived stability condition guarantees the required global convergence property with theoretical rigor. Further, in order to show clearly its distinctive features, we present how to design a formation controller for a class of multi-agent systems where each agent is modeled as a second-order system and is locally stabilized by the PD/PID controllers. For each cases, we also show that the formation stability can be easily analyzed based on the generalized Kalman-Yakubovich-Popov (KYP) lemma. Simulation examples illustrate its distinctive features and the achievement of a desired pursuit pattern.

Keywords: Multi-agent systems; Cooperative robot systems; Distributed control; Pursuit problems; Circulant matrices; Generalized Kalman-Yakubovich-Popov (KYP) lemma; Linear matrix inequality (LMI); Particle swarm optimization (PSO)

*Department of Information Physics and Computing, Graduate School of Information Science and Technology, The University of Tokyo, 7-3-1 Hongo, Bunkyo-ku, Tokyo, 113-8656, Japan. E-mail: Shinji.Hara@ipc.i.u-tokyo.ac.jp

†CREST, Japan Science and Technology Agency, 4-1-8 Honcho, Kawaguchi-shi, Saitama, 332-0012, Japan. E-mail: Kim.Tae.Hyoung@ipc.i.u-tokyo.ac.jp

‡Department of Mathematical Engineering and Information Physics, The University of Tokyo, 7-3-1 Hongo, Bunkyo-ku, Tokyo, 113-8656, Japan. E-mail: t60539@mail.ecc.u-tokyo.ac.jp

1 Introduction

Formation control which coordinates the motion of relatively simple and inexpensive multiple agents is one of the essential technologies that enable agents to cover a larger operational area and achieve complex tasks [7, 11]. Several research groups recently developed coordination control strategies which achieve an enclosing formation around a specific area (object) by multiple agents using local information (see [13, 7, 8, 6, 12] and the references therein). This type of coordination of motions is not only interesting but also significant, because it has many potential applications from an engineering standpoint as mentioned in Marshall et al. [7, 8] and Sepulchre et al. [12] For instance, it is useful when hazardous terrestrial/oceanographic exploration, military surveillance and rescue operation are performed by cooperative multi-agent systems.

Recently, Kim and Sugie [5] proposed a distributed on-line path planning scheme based on a modified cyclic pursuit strategy for target-enclosing operations by multi-agent systems. Despite its simple but particularly effective nature for target enclosing tasks, it could be a considerable drawback in real implementations that each agent is assumed to be a point mass with full actuation. That is, since agent's dynamics is not explicitly considered in path planning, their approach may suffer from the potential problem that each agent cannot track its designed trajectory precisely. In this case, the global convergence of multiple agents to the designated formation may not be achieved. It is therefore required for the improvement of its real implementability to develop a simple distributed on-line path planning strategy for multiple agents which generates the feasible trajectories under the explicit consideration of agent's dynamics and guarantees the global convergence property.

Regarding formation control with dynamic agents, Hara et al. [2] proposed a novel technique to analyze the characteristics of hierarchical large-scale linear systems. To this end, they first introduced the notion of a linear system with a generalized frequency variable; this system denoted as $\mathcal{G}(s)$ is developed by just replacing transfer function's 's' variable in the original system $L(s)$ with a rational function ' $\phi(s)$ ', i.e., $\mathcal{G}(s) := L(\phi(s))$. One of the examples of the systems which may retain generalized frequency variables is a class of formation control for multi-agent systems. Then, they developed a simple unified framework to analyze controllability, observability and stability of the hierarchical system $\mathcal{G}(s)$. Specifically, they presented the stability condition of $\mathcal{G}(s)$ in relation to the pole locations of $L(s)$ in the complex plane and the regions which $\phi(s)$ maps the right-half complex plane to. These results probably make a big contribution to the development of a cyclic pursuit based distributed on-line path planning scheme which guarantees the global convergence property with theoretical rigor.

This paper proposes a distributed cooperative control based on a cyclic pursuit strategy for target-enclosing operations by multiple agents. Here, it is assumed that n agents, which have common system dynamics and identical local controllers, are randomly dispersed in 3D space. The system of each agent combined with a controller is denoted by $H(s)$. In this paper, we first present an on-line path generator design method based on a cyclic pursuit scheme, which was proposed by Kim and Sugie [5]. Then, based on the results of Hara et al. [2], we derive a stability condition which the above cyclic pursuit based on-line path generator should satisfy to guarantee the formation stability. This is described in relation to the pole locations of the developed path generator in the complex plane and the region which $\phi(s)$ ($:= s/H(s)$) maps the right-half complex plane to. Further, in order to show clearly the distinctiveness and effectiveness of the proposed technique, we present an explicit stability condition for a cyclic pursuit based path generator combined with a class of multi-agent systems; each agent is modeled as a second-order system and is locally stabilized by the proportional-derivative (PD) or the proportional-integral-derivative (PID) controllers. For each cases, we first show that for given dynamic agents and on-line path generator, the formation stability can be readily analyzed based on the generalized Kalman-Yakubovich-Popov (GKYP) lemma [3, 4]. Then, both optimization based algebraic expression based approaches for the design of an on-line path generator, which satisfies theoretically the derived stability condition, are presented. Simulation examples illustrate its distinctive features and the achievement of a desired pursuit pattern.

The following notations will be used hereafter: For a Hermitian matrix, $M > 0$, $M \geq 0$, $M < 0$, and $M \leq 0$ denote positive definiteness, positive semidefiniteness, negative definiteness, and negative semidefiniteness, respectively. The transpose and complex conjugate transpose of the matrix M are denoted by M^T and M^* , respectively. The symbol \mathbf{H}_n denotes the set of $n \times n$ Hermitian matrices. The Kronecker product of matrices Γ and P is $\Gamma \otimes P$. The real and imaginary parts of a complex variable z is represented by $\text{Re}[z]$ and $\text{Im}[z]$, respectively.

2 System description and control aim

Consider a group of n agents dispersed in 3D space as shown in Figure 1. All agents are ordered from 1 to n ; i.e., P_1, P_2, \dots, P_n . We define P_{i+1} as prey agent of P_i . Denote the position vectors of the target object and the agent P_i ($i = 1, 2, \dots, n$) in the inertial frame by $\mathbf{p}_o(t) \in \mathbb{R}^3$ and $\mathbf{p}_i(t) \in \mathbb{R}^3$, respectively. It is assumed that an agent P_i can measure the following vectors:

$$\mathbf{d}_i (:= \mathbf{p}_i - \mathbf{p}_o), \quad \mathbf{a}_i (:= \mathbf{p}_i - \mathbf{p}_{i+1}). \quad (1)$$

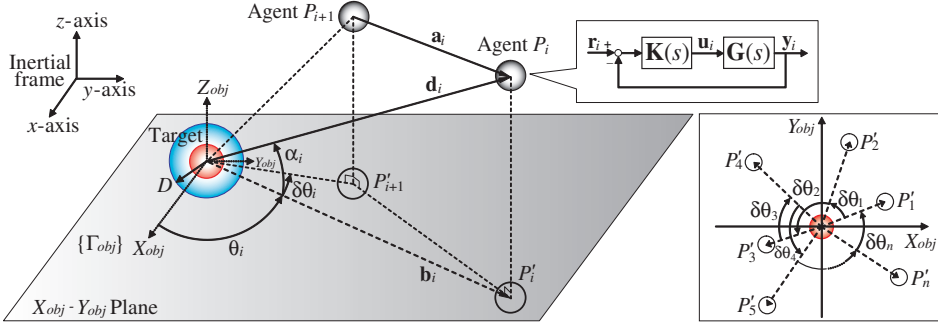


Figure 1: Coordinate frames and notations

Define the target-fixed frame $\{\Gamma_{obj}\}$ where the origin is at the center of target object, and X_{obj} -, Y_{obj} - and Z_{obj} -axes are parallel to x -, y - and z -axes of the inertial frame, respectively. Let \mathbf{b}_i denote the projected vector of \mathbf{d}_i onto the X_{obj} - Y_{obj} plane in the target-fixed frame, and define the following scalars:

$$\theta_i = \angle(\mathbf{e}_x, \mathbf{b}_i), \quad \alpha_i = \angle(\mathbf{b}_i, \mathbf{d}_i), \quad d_i := |\mathbf{d}_i|, \quad (2)$$

where \mathbf{e}_x denotes the unit vector in the X_{obj} -direction of $\{\Gamma_{obj}\}$, and $\angle(\mathbf{x}, \mathbf{y})$ denotes the counter-clockwise angle from the vector \mathbf{x} to the vector \mathbf{y} . Then, \mathbf{d}_i can be represented as $\mathbf{d}_i = [d_i \cos \theta_i \cos \alpha_i, d_i \sin \theta_i \cos \alpha_i, d_i \sin \alpha_i]^T$. Note that since $\mathbf{d}_{i+1} = \mathbf{d}_i - \mathbf{a}_i$, θ_{i+1} and $\delta\theta_i (:= \theta_{i+1} - \theta_i)$ can be calculated in a similar way based on (1). Let D denote the required distance between the target object and the agents.

Suppose that all agents P_i ($i = 1, 2, \dots, n$) have common system dynamics described by a MIMO plant as follows:

$$\mathbf{y}_i(s) := \begin{bmatrix} \theta_i(s) \\ d_i(s) \\ \alpha_i(s) \end{bmatrix} = \mathbf{G}(s) \mathbf{u}_i(s) := \begin{bmatrix} G_\theta(s) & 0 & 0 \\ 0 & G_d(s) & 0 \\ 0 & 0 & G_\alpha(s) \end{bmatrix} \mathbf{u}_i(s) \quad (3)$$

where $\mathbf{y}_i(s)$ is the system output, $\mathbf{u}_i(s)$ is the control input, and $\mathbf{G}(s)$ is the diagonal transfer matrix. Also, assume that all agents are locally stabilized by an identical diagonal feedback controller $\mathbf{K}(s)$ defined as $\mathbf{K}(s) := \text{diag}(K_\theta(s), K_d(s), K_\alpha(s))$ as illustrated in Figure 1. Therefore, θ -, d - and α -directional closed-loop transfer functions of each agent are described, respectively, as

$$H_\theta(s) = \frac{G_\theta(s)K_\theta(s)}{1+G_\theta(s)K_\theta(s)}, \quad H_d(s) = \frac{G_d(s)K_d(s)}{1+G_d(s)K_d(s)}, \quad H_\alpha(s) = \frac{G_\alpha(s)K_\alpha(s)}{1+G_\alpha(s)K_\alpha(s)}. \quad (4)$$

Now we consider how to form a geometric pattern for the target-enclosing operation by n agents. The detailed control objectives are stated as follows:

- (A1) n agents enclose the target object at uniformly spaced angle and maintain this angle.

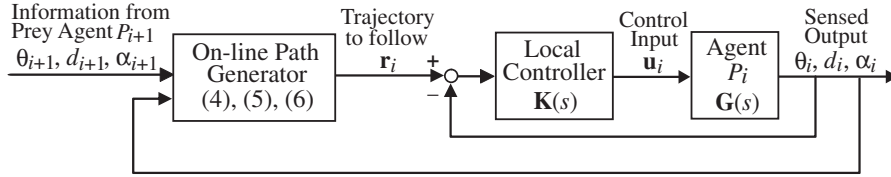


Figure 2: Formation controller configuration

- (A2) Each agent approaches to the target object and finally keeps the distance D .
- (A3) The angle α_i which corresponds to the altitude of each agent converges to the desired one Φ .

Note that for the sake of clarity, this paper only considers the equal convergence positions for all agents; i.e., $D_1 = D_2 = \dots = D_n = D$ and $\Phi_1 = \Phi_2 = \dots = \Phi_n = \Phi$, while the distinct ones for each agent can be assigned.

In the next section, the formation control scheme which achieves the objectives (A1)-(A3) is developed.

3 Distributed formation control based on a cyclic pursuit scheme

It is important from the practical viewpoint to achieve the desired global behavior through a relatively simple control law using only local information. As one of the feasible methods, we present a distributed cooperative control scheme motivated by a cyclic pursuit strategy for target-enclosing task [5], which realizes the required geometric formation mentioned in Section 2.

3.1 Design of a distributed on-line path generator

It is assumed that n agents are randomly dispersed in 3D space at the initial time instant as depicted in Figure 1, where $0 < |\delta\theta_i| < 2\pi$ for $i = 1, 2, \dots, n$, and $\sum_{i=1}^n \delta\theta_i = 2\pi$. Then, the distributed on-line path planning scheme for the i th agent P_i is described as (see Figure 2)

$$\dot{\theta}_i(t) = k_1 \delta\theta_i(t), \quad (5)$$

$$\dot{d}_i(t) = k_2 (D - d_i(t)), \quad (6)$$

$$\dot{\alpha}_i(t) = k_3 (\Phi - \alpha_i(t)), \quad (7)$$

where k_1 , k_2 , and k_3 (> 0) are design parameters,

$$\begin{cases} \delta\theta_i(t) := \theta_{i+1}(t) - \theta_i(t), & i = 1, 2, \dots, n-1 \\ \delta\theta_n(t) := \theta_1(t) - \theta_n(t) + 2\pi, & i = n. \end{cases}$$

It is important to note that the gains k_1 , k_2 , and k_3 should satisfy some conditions to guarantee the achievement of the desired global formation (A1)-(A3), which will be explained later in detail. Then, the reference position $\mathbf{r}_i(t) = [r_i^1(t), r_i^2(t), r_i^3(t)]^T := [\theta_i(t), d_i(t), \alpha_i(t)]^T$ for the i th agent shown in Figure 1 is designed by (5), (6) and (7).

Note that, in the proposed path planning method, each agent individually decides its reference position based on the local information on only one other agent and the target object, which is probably minimum. Further, it has additional distinctive features as follows: each agent individually obtains the required information using the sensor systems implemented on its body, which means that no centralized communication mechanism between agents is introduced. Also, it is a memoryless controller in the sense that each agent determines the next behavior based only on the current position of its prey, independently of the past behavior of its prey. Thus, it is an easily implementable method from the engineering viewpoint.

Now, the control objectives (A1)-(A3) in Section 2 can be formulated algebraically as follows:

$$(A1') \quad \delta\theta_i(t) \rightarrow 2\pi/n[\text{rad}] \text{ as } t \rightarrow \infty,$$

$$(A2') \quad d_i(t) \rightarrow D \text{ as } t \rightarrow \infty,$$

$$(A3') \quad \alpha_i(t) \rightarrow \Phi[\text{rad}] \text{ as } t \rightarrow \infty,$$

for $i = 1, 2, \dots, n$. It has been proved in Kim and Sugie [5] that path planning schemes (5)-(7) can achieve the above control objectives (A1')-(A3') under the assumption that each agent in the group is supposed to be a point mass. However, when agent's dynamics is considered explicitly, the achievement of the stable global formation (A1')-(A3') cannot be guaranteed only by the condition that k_1 , k_2 and k_3 in (5)-(7) are positive real numbers. The following example illustrates this fact clearly.

Example 1. In this example, we investigate only the θ -directional behaviors of $n = 9$ agents for the sake of clarity. The initial values of $\theta_i(t)$ [rad] are set as follows:

$$\begin{aligned} \theta_1 = 0.198, \theta_2 = 1.269, \theta_3 = 0.050, \theta_4 = 1.491, \theta_5 = 1.175, \\ \theta_6 = 0.189, \theta_7 = 2.045, \theta_8 = 0.793, \theta_9 = 1.712. \end{aligned} \quad (8)$$

Assume that the common θ -directional agent dynamics $G_\theta(s)$ and its stabilizing PD controller $K_\theta(s)$ are, respectively, given as

$$G_\theta(s) = \frac{1}{s(s+3)}, \quad K_\theta(s) = 5 + 2s. \quad (9)$$

The reference position $r_i^1(t)$ ($= \theta_i(t)$) for agent i is designed based on (5) with $k_1 = 1.5$. The simulation is performed for $t = 5$ [sec]. The changes of

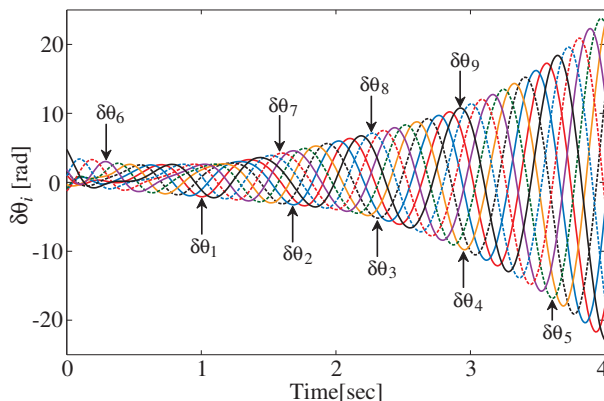


Figure 3: Plot showing the divergence of the relative angles $\delta\theta_i$ ($i = 1, 2, \dots, 9$)

$\delta\theta_i(t)$ ($i = 1, 2, \dots, 9$) with respect to time are plotted in Figure 3. It shows clearly that any $\delta\theta_i$ does not converge to $2\pi/9[\text{rad}]$. ■

From the above observation, one can see that, in order to achieve the global formation (A1')-(A3'), three gains k_1 , k_2 and k_3 should be set carefully. Hence, in the following subsection, we provide a simple and unified theoretical framework showing how to determine k_1 , k_2 and k_3 in relation to agent's dynamics $H_\theta(s)$, $H_d(s)$ and $H_\alpha(s)$, respectively.

3.2 Formation stability analysis

In the following, it is supposed for the sake of clarity that $G_\theta(s) = G_d(s) = G_\alpha(s) = G(s)$ and $K_\theta(s) = K_d(s) = K_\alpha(s) = K(s)$, while the distinct case can be handled. Thus, under the above assumptions, θ -, d - and α -directional closed-loop transfer functions of each agent become identical as $H_\theta(s) = H_d(s) = H_\alpha(s) = H(s)$. In order to analyze the formation stability of multi-agent systems considered in Section 3.1, we rewrite (5) in the following vector form:

$$\dot{\boldsymbol{\theta}}(t) = A_\theta \boldsymbol{\theta} + B_\theta \quad (10)$$

with

$$\begin{aligned} A_\theta &:= \text{circ}(-k_1, k_1, 0, 0, \dots, 0) \in \mathbb{R}^{n \times n}, \\ B_\theta &:= [0, 0, \dots, 0, 2k_1\pi]^T \in \mathbb{R}^n, \end{aligned} \quad (11)$$

where $\boldsymbol{\theta} := [\theta_1, \theta_2, \dots, \theta_n]^T \in \mathbb{R}^n$ and circ denotes the circulant matrix. Thus, the overall $\boldsymbol{\theta}$ -directional control scheme can be depicted as shown in Figure 4, where $\hat{H}(s) := (1/s)H(s)$ and $\mathbf{r}^1 := [r_1^1, r_2^1, \dots, r_n^1]^T \in \mathbb{R}^n$. Here, it is assumed that $\hat{H}(s)$ is strictly proper. In the same manner, (6) and (7)

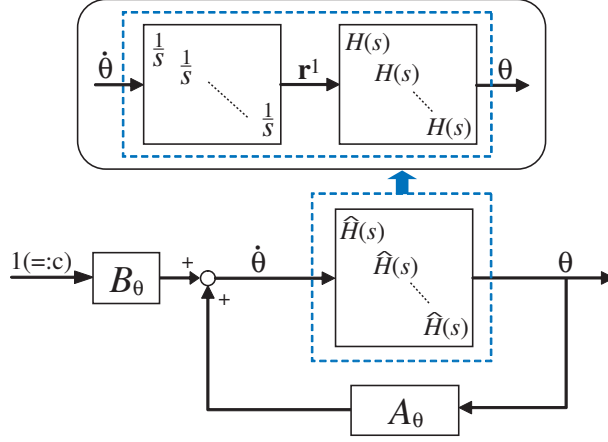


Figure 4: Block diagram of the θ -directional formation controlled system

can be written, respectively, as

$$\dot{\mathbf{d}}(t) = A_d \mathbf{d}(t) + B_d, \quad (12)$$

$$\dot{\boldsymbol{\alpha}}(t) = A_\alpha \boldsymbol{\alpha}(t) + B_\alpha, \quad (13)$$

with $\mathbf{d} := [d_1, d_2, \dots, d_n]^T \in \mathbb{R}^n$, $\boldsymbol{\alpha} := [\alpha_1, \alpha_2, \dots, \alpha_n]^T \in \mathbb{R}^n$, $A_d := -\text{diag}(k_2, k_2, \dots, k_2) \in \mathbb{R}^{n \times n}$, $A_\alpha := -\text{diag}(k_3, k_3, \dots, k_3) \in \mathbb{R}^{n \times n}$, $B_d := (k_2 D) \mathbf{1}_n \in \mathbb{R}^n$, $B_\alpha := (k_3 \Phi) \mathbf{1}_n \in \mathbb{R}^n$ where $\mathbf{1}_n := [1, 1, \dots, 1]^T \in \mathbb{R}^n$. The block diagrams of the \mathbf{d} - and $\boldsymbol{\alpha}$ -directional formation controlled systems have the same form with that in Figure 4. Thus, for the sake of page limitation, we mainly consider the θ -directional control strategy.

On the other hand, it is important to note that A_θ always has exactly one zero eigenvalue, while the remaining $n - 1$ eigenvalues lie strictly in the left-half complex plane (for details, see Section 4.2 and Kim and Sugie [5]). It means that $\dot{\boldsymbol{\theta}}$ converges to the null space $\{\boldsymbol{\sigma} | \boldsymbol{\sigma} = \sigma I_n, \sigma \in \mathbb{R}\}$ where $I_n = [1, 1, \dots, 1]^T \in \mathbb{R}^n$; i.e., $\dot{\theta}_1 = \dot{\theta}_2 = \dots = \dot{\theta}_n$. Then, it results in $\delta\theta_1 = \delta\theta_2 = \dots = \delta\theta_n = 2\pi/n$ in the steady state, which implies the formation stability described in Section 3.1. Therefore, we can disregard exactly one zero eigenvalue and determine the formation stability based on the remaining $n - 1$ eigenvalues of A_θ [5, 7, 13]. Based on the above facts, we consider hereafter only $n - 1$ eigenvalues of A_θ except for one zero eigenvalue, if no confusion could arise.

In Figure 4, the transfer function $\mathcal{G}_\theta(s)$ from c to $\boldsymbol{\theta}$ is obtained as

$$\mathcal{G}_\theta(s) = \left(\frac{1}{\hat{H}(s)} I_n - A_\theta \right)^{-1} B_\theta = \mathcal{F}_u \left(\begin{bmatrix} A_\theta & B_\theta \\ I_n & 0 \end{bmatrix}, \hat{H}(s) I_n \right) \quad (14)$$

where \mathcal{F}_u denotes the upper linear fractional transformation (LFT). By considering the transfer function

$$L_\theta(s) = (sI_n - A_\theta)^{-1}B_\theta \quad (15)$$

which is also written as $L_\theta(s) \sim (A_\theta, B_\theta, I_n, 0)$, it follows from (14) that

$$\mathcal{G}_\theta(s) = L_\theta(\phi(s)), \quad \phi(s) := 1/\hat{H}(s). \quad (16)$$

Note that the variable ‘ s ’ in (15) characterizes the frequency properties of the transfer function $L_\theta(s)$ and that $\mathcal{G}_\theta(s)$ is generated by just replacing ‘ s ’ by ‘ $\phi(s)$ ’ in $L_\theta(s)$. Hence, we say that the transformed transfer function $\mathcal{G}_\theta(s) = L_\theta(\phi(s))$ of $L_\theta(s)$ has a generalized frequency variable $\phi(s)$ (see Hara et al. [2] for details). The transfer functions $\mathcal{G}_d(s)$, $L_d(s)$, $\mathcal{G}_\alpha(s)$ and $L_\alpha(s)$ can be derived in a similar manner.

Next, in order to derive a formation stability condition for the system $\mathcal{G}_\theta(s)$ in (14), we first describe a key result on stability analysis of $\mathcal{G}_\theta(s)$ developed by Hara et al. [2]. In their paper, instead of Nyquist’s graphical stability test given in Fax and Murray [1], the domain in terms of the poles of the path generator’s dynamics $L_\theta(s)$ such that $\mathcal{G}_\theta(s) = L_\theta(\phi(s))$ is stable is derived. Before we proceed, the notations which will be used throughout this paper are introduced: the domains Ω_+ and Ω_+^c in the complex plane are defined as

$$\Omega_+ := \phi(\mathbb{C}_+), \quad \Omega_+^c := \mathbb{C} \setminus \Omega_+, \quad (17)$$

where $\mathbb{C}_+ = \{s \in \mathbb{C} : \text{Re}[s] \geq 0\}$. Since $\Omega_+ = \{\lambda \in \mathbb{C} : \exists s \in \mathbb{C}_+ \text{ such that } \phi(s) = \lambda\}$, it follows that Ω_+^c can be alternatively expressed as $\Omega_+^c = \{\lambda \in \mathbb{C} : \forall s \in \mathbb{C}_+, \phi(s) \neq \lambda\}$. Then, the following lemma describes a sufficient condition for the existence of A_θ (A_d , A_α) so that the hierarchical system $\mathcal{G}_\theta(s)$ ($\mathcal{G}_d(s)$, $\mathcal{G}_\alpha(s)$) is stable for a given $\hat{H}(s)$.

Lemma 1 *Suppose that $\hat{H}(s)$ is stable or that $\hat{H}(s)$ does not possess non-minimum phase zeros. Then, there exists A_θ (A_d , A_α) such that $\mathcal{G}_\theta(s) = L_\theta(\phi(s))$ ($\mathcal{G}_d(s) = L_d(\phi(s))$, $\mathcal{G}_\alpha(s) = L_\alpha(\phi(s))$) is stable.*

Next, the key theorem which describes the conditions for controllability, observability and stability of $\mathcal{G}_\theta(s)$, $\mathcal{G}_d(s)$ and $\mathcal{G}_\alpha(s)$ are provided as follows:

Theorem 1 *Consider the linear systems $\mathcal{G}_\theta(s)$ in (14) and $L_\theta(s)$ in (15), and the generalized frequency variable $\phi(s)$ in (16). Assume that $\hat{H}(s)$ is strictly proper. Then, $\mathcal{G}_\theta(s)$ ($\mathcal{G}_d(s)$, $\mathcal{G}_\alpha(s)$) is controllable and observable if and only if $L_\theta(s)$ ($L_d(s)$, $L_\alpha(s)$) and $\hat{H}(s)$ are both controllable and observable. Further, $\mathcal{G}_\theta(s) = L_\theta(\phi(s))$ ($\mathcal{G}_d(s) = L_d(\phi(s))$, $\mathcal{G}_\alpha(s) = L_\alpha(\phi(s))$) is stable if and only if all the poles of $L_\theta(s)$ (L_d , L_α) belong to Ω_+^c in (17).*

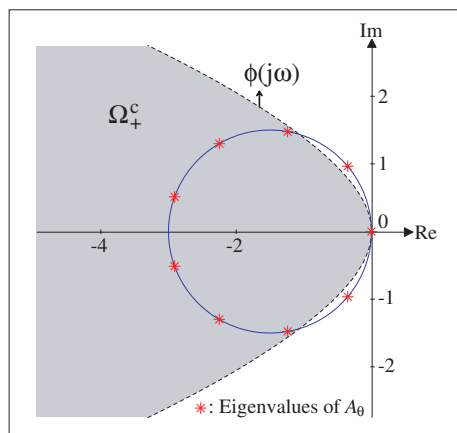


Figure 5: The domain Ω_+^c and the eigenvalues of A_θ

Its proof can be found in Hara et al. [2]. The above theorem means that the stability of $\mathcal{G}_\theta(s)$ can be judged by just looking at the locations of eigenvalues of A_θ in relation to a domain Ω_+^c which is determined by using $\hat{H}(s)$. It is important to note from Lemma 1 and Theorem 1 that for the case where $\hat{H}(s)$ does not possess non-minimum phase zeros, there exists a domain Ω_+^c containing the origin, and the eigenvalues of A_θ (A_d and A_α) can be placed in this domain (for details, see Hara et al. [2]).

Finally, we present the following theorem which says that the global formation stability (i.e., (A1'), (A2') and (A3')) is guaranteed as long as $n - 1$ poles of $L_\theta(s)$ (except for one zero pole) and all the poles of $L_d(s)$ and $L_\alpha(s)$ belong to a domain Ω_+^c .

Theorem 2 *Consider the system of n dynamic agents. It is assumed that all agents are randomly dispersed in 3D space at the initial time instant as shown in Figure 1, where $0 < |\delta\theta_i| < 2\pi$ for $i = 1, 2, \dots, n$, and $\sum_{i=1}^n \delta\theta_i = 2\pi$. Also, suppose that (i) $n - 1$ poles of $L_\theta(s)$ (except for one zero pole) belongs to Ω_+^c , (ii) all the poles of $L_d(s)$ and $L_\alpha(s)$ belong to Ω_+^c . Then, the path planning schemes (5)-(7) achieve the formation stability (A1')-(A3') simultaneously.*

This fact can be easily proved based on the result of Kim and Sugie [5]. The above theorem shows how to determine k_1 , k_2 and k_3 of (5)-(7) in order to guarantee that all agents assemble into the desired formation around the target object in 3D space. For example, consider the multi-agent system given in Example 1, where k_1 was set as $k_1 = 0.85$. In that case, the pole locations of $L_\theta(s)$ and the domain Ω_+^c are as illustrated in Figure 5. It verifies that two poles of $L_\theta(s)$ (except for one zero pole) do not belong to Ω_+^c . Consequently, one reaches the conclusion that (A1') cannot be achieved, which is evident from Figure 3.

4 Target-enclosing formation control for a class of multi-agent systems: PD controller case

In this section, we provide a constructive methodology that describes the domain Ω_+^c in the complex plane when the transfer function $\hat{H}(s)$ is specified. Further, we present how to design k_1 , k_2 and k_3 in (5)-(7) guaranteeing that $n - 1$ poles of $L_\theta(s)$ and all the poles of $L_d(s)$ and $L_\alpha(s)$ belong to Ω_+^c .

4.1 Multi-agent systems stabilized by PD controllers

It is assumed that θ -, d - and α -directional agent dynamics are identical; i.e.,

$$G(s) = \frac{\zeta}{s(s + \xi)} \quad (18)$$

where $\zeta > 0$. Then, the PD controller $K_{PD}(s)$ such as

$$K_{PD}(s) = k_p(1 + t_d s) \quad (19)$$

is introduced to stabilize (18). Hence, it follows from $G(s)$ in (18) and $K_{PD}(s)$ in (19) that

$$H(s) = \frac{\zeta k_p t_d s + \zeta k_p}{s^2 + (\xi + \zeta k_p t_d) s + \zeta k_p} = \frac{t_d s + 1}{(1/\zeta k_p) s^2 + ((\xi/\zeta k_p) + t_d) s + 1}. \quad (20)$$

Let $\tilde{s} = t_d s$. Then, (20) can be modified as

$$H(\tilde{s}) = \frac{\tilde{s} + 1}{\frac{1}{\zeta k_p t_d^2} \tilde{s}^2 + \left(\frac{\xi}{\zeta k_p t_d} + 1\right) \tilde{s} + 1} = \frac{\tilde{s} + 1}{a \tilde{s}^2 + b \tilde{s} + 1} \quad (21)$$

where $a := 1/(\zeta k_p t_d^2) (> 0)$ and $b := \xi/(\zeta k_p t_d) + 1$. Therefore, without loss of generality, the following form of the generalized frequency variable $\phi(s)$ can be considered hereafter:

$$\phi(s) = \frac{1}{\hat{H}(s)} = \frac{s}{H(s)} = \frac{as^3 + bs^2 + s}{s + 1}. \quad (22)$$

Here, $H(s)$ is stable if and only if $b > 0$, since $a > 0$.

Next, we characterize the domains Ω_+ and Ω_+^c in the complex plane. These regions are partitioned by the image of $\phi(j\omega)$ in (22) where $\omega \in \mathbb{R}$. In order to illustrate Ω_+^c clearly, we first define the real and the imaginary parts, $f(\omega)$ and $g(\omega)$, of $\phi(j\omega)$ in (22) as

$$f(\omega) := \text{Re}[\phi(j\omega)] = \frac{\omega^2(1 - b - a\omega^2)}{1 + \omega^2}, \quad (23)$$

$$g(\omega) := \text{Im}[\phi(j\omega)] = \frac{\omega(1 + (b - a)\omega^2)}{1 + \omega^2}. \quad (24)$$

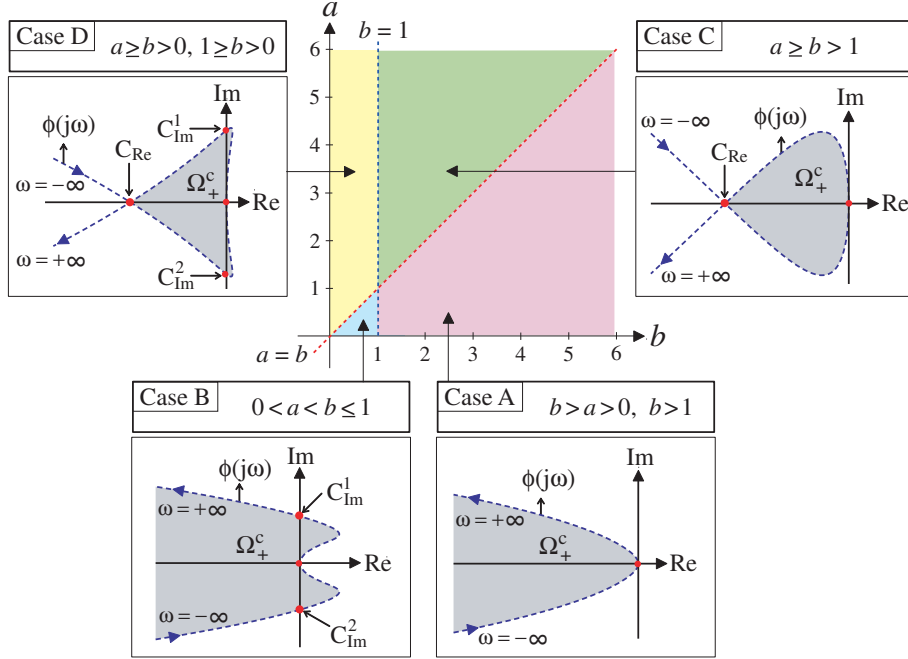


Figure 6: The image of $\phi(j\omega)$ and the domain Ω_+^c

The crossing points of $\phi(j\omega)$ and the imaginary axis can be easily obtained by finding ω_I which satisfies $f(\omega_I) = 0$ and then calculating $g(\omega_I)$. Similarly, the crossing points of $\phi(j\omega)$ and the real axis are obtained from $f(\omega_R)$ where ω_R satisfies $g(\omega_R) = 0$. In this case, depending on the signs of $1 - b$ and $a - b$, the image of $\phi(j\omega)$ yields four types of diagrams as shown in Figure 6. In this figure, C_{Im}^1 and C_{Im}^2 are determined as

$$C_{\text{Im}}^{1,2} = g(\omega_I^{1,2}) = \pm b \left(\frac{1-b}{a} \right)^{1/2}, \quad \omega_I^{1,2} = \pm \left(\frac{1-b}{a} \right)^{1/2} \in \mathbb{R}, \quad (25)$$

if $0 < b \leq 1$, which is equivalent to $\xi \leq 0$. On the other hand, C_{Re} is

$$C_{\text{Re}} = f(\omega_R^{1,2}) = \frac{b}{b-a}, \quad \omega_R^{1,2} = \pm \frac{1}{(a-b)^{1/2}} \in \mathbb{R}, \quad (26)$$

if $a \geq b > 0$.

In the following subsection, a considerably simple way to judge whether nonzero $n - 1$ poles of $L_\theta(s)$ with a given k_1 belong to Ω_+^c in Figure 6 or not.

4.2 Algebraic formation stability criteria

It is important to note that since A_θ is a circulant matrix, its eigenvalues can be written in the following complex form (see Kim and Sugie [5] for

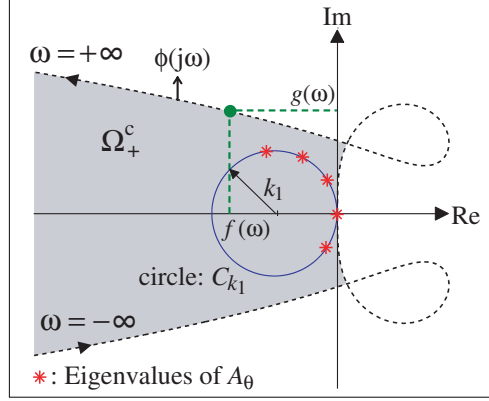


Figure 7: The eigenvalues λ_i ($i = 1, 2, \dots, n$) of A_θ and the domain Ω_+^c

details):

$$\lambda_i = k_1 \left[\cos \left(\frac{2\pi(i-1)}{n} \right) - 1 \right] + jk_1 \sin \left(\frac{2\pi(i-1)}{n} \right). \quad (27)$$

Since $k_1 > 0$, A_θ has exactly one zero eigenvalue, λ_1 , while the remaining nonzero $n - 1$ eigenvalues λ_i , $i = 2, 3, \dots, n$, lie strictly in the left-half complex plane; i.e., these are located on the circumference of radius k_1 whose center is at $(-k_1, 0)$ as illustrated in Figure 7. Note that $\lambda_1 = 0$ has the consequence that angular velocities $\dot{\theta}_i$ of all agents around Z_{obj} -axis converge to the same value; i.e., $\dot{\theta}_1 = \dot{\theta}_2 = \dots = \dot{\theta}_n$ as mentioned in Section 3.2.

Now assume that k_1 is given by the designer. Then, one can easily find that if the following condition is satisfied,

$$(\phi(j\omega) + k_1)^*(\phi(j\omega) + k_1) > k_1^2, \quad \forall \omega \in \mathbb{R} \setminus \{0\}, \quad (28)$$

then nonzero $n - 1$ eigenvalues λ_i ($i = 2, 3, \dots, n$) of A_θ are placed in the domain Ω_+^c . The inequality condition (28) is rewritten as $1 + k_1 \hat{H}^*(j\omega) + k_1 \hat{H}(j\omega) > 0$ by using $\phi(j\omega) = 1/\hat{H}(j\omega)$. Therefore, we can see that (28) is equivalent to the following inequality condition:

$$L(\omega) := -2\text{Re}[\hat{H}(j\omega)] = \frac{2(a\omega^2 + b - 1)}{a^2\omega^4 + (b^2 - 2a)\omega^2 + 1} < \frac{1}{k_1} \quad (29)$$

for $\forall \omega \in \mathbb{R} \setminus \{0\}$. The condition in (29) implies that if a given k_1^{-1} is bigger than the maximum value of $L(\omega)$ (except at $\omega = 0$), then nonzero $n - 1$ eigenvalues λ_i ($i = 2, 3, \dots, n$) of A_θ are placed in the domain Ω_+^c . From the above observations, the following result which specifies the maximum permissible limit of a gain $k_1 (> 0)$ is obtained.

Theorem 3 Let L_{\max_0} and L_{\max_1} be defined, respectively, as

$$L_{\max_0} := 2(b-1), \quad L_{\max_1} := \frac{2(a\hat{\omega} + b - 1)}{a^2\hat{\omega}^2 + (b^2 - 2a)\hat{\omega} + 1}, \quad (30)$$

where

$$\hat{\omega} = \frac{1-b}{a} + \frac{b}{a^2} \sqrt{a(a-b+1)}. \quad (31)$$

Suppose that a given gain $k_1 (> 0)$ in (5) satisfies the following condition:

- (i) $k_1 < L_{\max_1}^{-1}$, if $\hat{\omega}$ is a positive real number and $L_{\max_1} \geq L_{\max_0}$,
- (ii) $k_1 \leq L_{\max_0}^{-1}$, otherwise.

Then, nonzero $n-1$ eigenvalues λ_i ($i = 2, 3, \dots, n$) of A_θ in (27) are placed in the domain Ω_+^c .

Proof. We first find the maximum value of $L(\omega)$. It follows from (29) that

$$\frac{dL(\omega)}{d\omega} = \frac{-4\omega(a^3\omega^4 + 2a^2(b-1)\omega^2 + b^3 - b^2 - 2ab + a)}{(a^2\omega^4 + (b^2 - 2a)\omega^2 + 1)^2}. \quad (32)$$

Hence, ω satisfying $\frac{dL(\omega)}{d\omega} = 0$ is obtained as

$$\omega_0 = 0, \quad \omega_{1,2}^2 = \frac{1-b}{a} \pm \frac{b}{a^2} \sqrt{a(a-b+1)}. \quad (33)$$

Note that ω_1 (or ω_2) can be a solution of $\frac{dL(\omega)}{d\omega} = 0$ only if ω_1^2 (or ω_2^2) is a positive real number. Next, we show that ω_2 is a trivial solution. The condition (28) can be written by using (23)-(24) as $(f(\omega) + k_1)^2 + g^2(\omega) > k_1^2$. It is self-evident that if $f(\omega) \geq 0$, the above condition is satisfied for any $k_1 (> 0)$. Hence, it is enough to check whether (29) is guaranteed for ω satisfying

$$\omega^2 > \frac{1-b}{a} =: \omega_f, \quad (34)$$

which is obtained from $f(\omega) < 0$. It then follows from $\omega_2^2 \in \mathbb{R}$ in (33) and ω_f in (34) that $\omega_2^2 \leq \omega_f$, since $b > 0$ from the stability condition of $H(s)$. Therefore, ω_2 is a trivial solution, and the maximum value of $L(\omega)$ is determined by ω_0 or $\omega_1 (= \pm\sqrt{\hat{\omega}})$. From the above results, we can see that the condition (29) is guaranteed if $k_1^{-1} > L(\omega_1) (= L_{\max_1})$ holds where ω_1^2 is a positive real number and $L(\omega_1) \geq L(\omega_0) (= L_{\max_0})$, which proves (i). On the other hand, if (a) $\omega_1^2 \notin \mathbb{R}$ or (b) $\omega_1^2 \in \mathbb{R}$ and $L(\omega_1) < L(\omega_0)$, then the maximum of $L(\omega)$ is determined by $\omega = \omega_0 (= 0)$. It implies that if $k_1^{-1} \geq L(\omega_0)$ is satisfied, then $k_1^{-1} > L(\omega)$ is guaranteed for $\forall \omega \in \mathbb{R} \setminus \{0\}$, which proves (ii). \square

Some plots of $L(\omega)$ for various a and b are illustrated in Figure 8. This figure

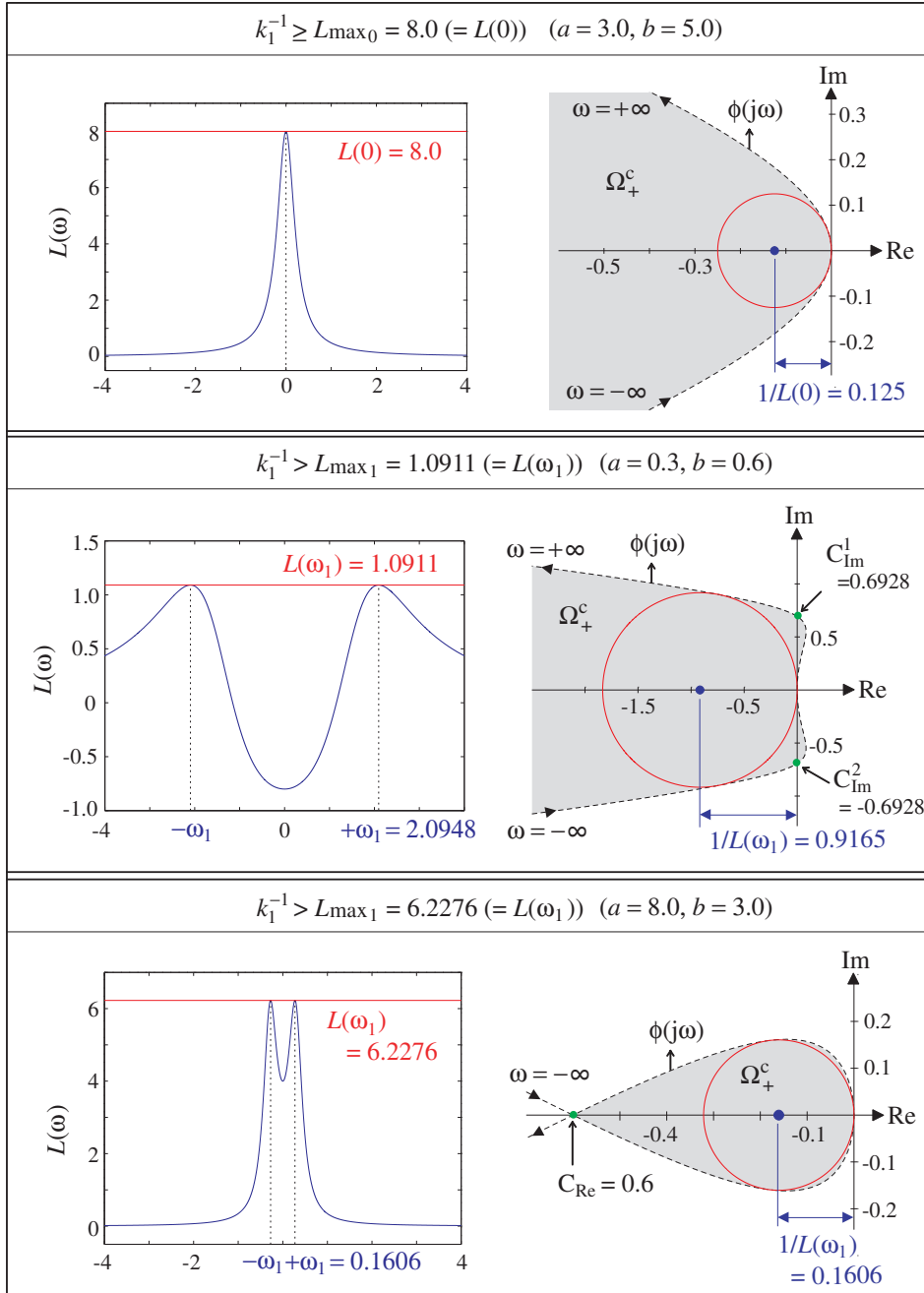


Figure 8: Plots of $L(\omega)$ for various $a(> 0)$ and $b(> 0)$

illustrates that the maximum value of $L(\omega)$ is determined by $L(0)(=L_{\max_0})$ or $L(\omega_1)(=L_{\max_1})$.

Next, we consider the conditions for $k_2(> 0)$ and $k_3(> 0)$ in (6)-(7). Note that matrices A_d and A_α in (12)-(13) are written as

$$A_d = -\text{diag}(k_2, k_2, \dots, k_2) \in \mathbb{R}^{n \times n}, \quad (35)$$

$$A_\alpha = -\text{diag}(k_3, k_3, \dots, k_3) \in \mathbb{R}^{n \times n}. \quad (36)$$

Thus, the eigenvalues of A_d and A_α are, respectively, $-k_2$ and $-k_3$, which implies that all eigenvalues are negative real numbers. Based on the above observations and Figure 6, the following theorem which specifies the maximum permissible limits of $k_2(> 0)$ and $k_3(> 0)$ are obtained.

Theorem 4 *Suppose that gains k_2 and k_3 in (6)-(7) satisfy the following condition:*

- (i) $\frac{b}{b-a} < -k_2 < 0$ and $\frac{b}{b-a} < -k_3 < 0$, if $a \geq b$,
- (ii) $k_2 > 0$ and $k_3 > 0$, otherwise.

Then, all eigenvalues of A_d and A_α in (12)-(13) are placed in the domain Ω_+^c .

Proof. First, consider the case that given a and b satisfy $a \geq b$. In this case, the crossing point $C_{\text{Re}}(< 0)$ of $\phi(j\omega)$ and the imaginary axis exists, which can be verified from (26) and Figure 6 (see Cases C and D). Hence, in order that all eigenvalues of A_d , $-k_2$, are placed in the domain Ω_+^c , k_2 should guarantee $C_{\text{Re}} < -k_2 < 0$, which is also the case of k_3 . On the other hand, if a and b satisfy $a < b$, then $\phi(j\omega)$ does not cross the imaginary axis (see Cases A and B in Figure 6). It means that k_2 and k_3 can take any positive real numbers in these cases. \square

4.3 Optimization-based design of path generator

In this subsection, we present another method to determine k_1 in (5) which guarantees that nonzero $n - 1$ poles of $L_\theta(s)$ belong to Ω_+^c in Figure 6. Note that the following condition

$$(f(\omega) + k_1)^2 + g^2(\omega) > k_1^2, \quad \forall \omega \in \mathbb{R} \setminus \{0\} \quad (37)$$

is equivalent to the inequality condition in (28). Therefore, the maximum of k_1 ($k_{1,\max}$), which guarantees that a circle C_{k_1} in Figure 7 exists inside the domain $\Omega_+^c \cup \Omega_b$ where $\Omega_b := \phi(j\mathbb{R})$, can also be readily found by solving the optimization problem:

[Constrained optimization problem]

For $f(\omega)$ in (23) and $g(\omega)$ in (24), solve

$$k_{1,\max} := \arg \max_{k_1, \omega} k_1 \quad (38)$$

subject to $k_1 > 0$ and

$$(f(\omega) + k_1)^2 + g^2(\omega) \geq k_1^2 \quad (39)$$

where the search range of $\omega \in \mathbb{R}$ is specified as follows:

- (i) $\omega > 0$ for Case A,
- (ii) $\omega_I^1 \leq \omega$ for Case B,
- (iii) $0 < \omega \leq \omega_R$ ($\omega_R > 0$) for Case C,
- (iv) $\omega_I^1 \leq \omega \leq \omega_R$ ($\omega_R > 0$) for Case D.

Hence, if k_1 in (5) is set as $0 < k_1 < k_{1,\max}$, then all nonzero poles of $L_\theta(s)$ belong to Ω_+^c illustrated in Figure 6. Table 1 verifies that $1/k_{1,\max}$ obtained by solving (38)-(39) and the maximum value of $L(\omega)$ in (29) are identical, where the optimization problem is solved through the constrained particle swarm optimization method proposed by Maruta et al. [9, 10].

Example 2. To illustrate the dynamic performance of the proposed distributed cooperative control scheme, a simulation is carried out. Here, $n = 9$ agents are randomly dispersed in 3D space at first and finally should achieve the required formation stated in Section 2. Specifically, the desired formation is chosen to be given by $\delta\theta_i = 2\pi/9[\text{rad}]$ ($i = 1, 2, \dots, 9$), $D = 5$ and $\Phi = 0[\text{rad}]$. The initial values of $\alpha_i(t)[\text{rad}]$ and $d_i(t)$ are set as follows:

$$\begin{aligned} \alpha_1 = \alpha_5 = 1.484, \quad \alpha_2 = \alpha_6 = 1.222, \quad \alpha_3 = 0.596, \\ \alpha_4 = 1.047, \quad \alpha_7 = 0.698, \quad \alpha_8 = 1.396, \quad \alpha_9 = 0.960, \end{aligned} \quad (40)$$

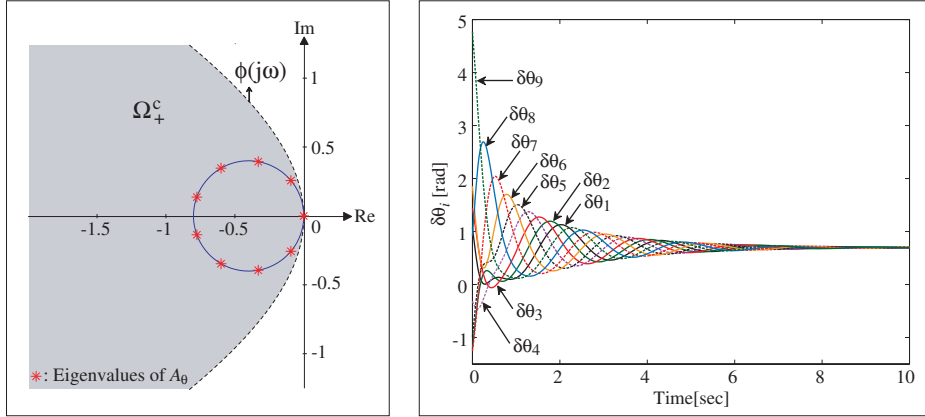
and

$$d_1 = d_6 = 30, \quad d_2 = d_7 = 25, \quad d_3 = 13, \quad d_4 = d_8 = 20, \quad d_5 = d_9 = 15. \quad (41)$$

The initial values of $\theta_i(t)$ are identical to those of Example 1. Let $G(s)$ and $K(s)$ be identical, respectively, to $G_\theta(s)$ and $K_\theta(s)$ in (9); i.e., $G(s) =$

Table 1: The value of $1/k_{1,\max}$ obtained by (38)-(39) and the maximum value of $L(\omega)$ in (29).

	Case A	Case B	Case C	Case D
a, b	3, 5	0.3, 0.6	8, 3	2, 0.5
$1/k_{1,\max}$	8.0	1.0911	6.2276	8.2293
Maximum value of $L(\omega)$	8.0	1.0911	6.2276	8.2293



(a) Domain Ω_+^c and nine eigenvalues of A_θ with $k_1 = 0.4$ (b) Plot showing the convergence of the relative angles $\delta\theta_i$ ($i = 1, 2, \dots, 9$)

Figure 9: Plots showing the global formation stability in Example 2.

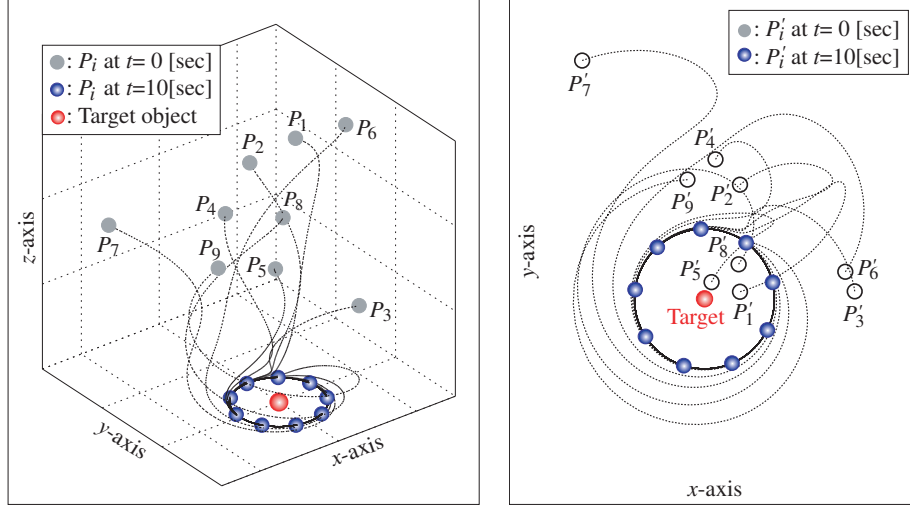
$1/s(s+3)$ and $K(s) = 5 + 2s$. Hence, the image of $\phi(j\omega)$ ($:= s(1 + G(s)K(s))/G(s)K(s)$) corresponds to Case A in Figure 6 ($a = 1.25$, $b = 2.5$). Consequently, we set $0 < k_1 = 0.4 < k_{1,\max} = 0.8333$, $k_2 = 0.3 > 0$ and $k_3 = 0.3 > 0$. Here, $k_{1,\max}$ is obtained through the constrained particle swarm optimization method proposed by Maruta et al. [9, 10]. Eight nonzero eigenvalues of A_θ belong to the domain Ω_+^c , which is confirmed in Figure 9(a). Figure 10(a) illustrates the resulting position trajectories of nine agents during the simulation: all agents converge to a circular formation around the target object and maintain the form of an equilateral and equiangular polygon. The changes of $\delta\theta_i$ with respect to time are plotted in Figure 9(b), where $\delta\theta_i$ finally converges to $2\pi/9$ [rad]. These results clearly demonstrate that the control goals (A1')-(A3') mentioned in Section 3 are achieved. ■

5 Target-enclosing formation control for a class of multi-agent systems: PID controller case

In this section, we consider the case that each agent is stabilized by the PID controller $K_{\text{PID}}(s)$ such as

$$K_{\text{PID}}(s) = k_p \left(1 + \frac{1}{t_i s} + t_d s \right), \quad (42)$$

where $k_p(> 0)$, $t_i(> 0)$ and $t_d(> 0)$ denote proportional gain, integral and derivative times, respectively. Hence, it follows from $G(s)$ in (18) and



(a) Position trajectories of agents P_i ($i = 1, 2, \dots, 9$) (b) Planar trajectories of agents P_i ($i = 1, 2, \dots, 9$) converging to the desired formation

Figure 10: Simulation results of Example 2.

$K_{\text{PID}}(s)$ in (42) that

$$H(s) = \frac{t_d t_i s^2 + t_i s + 1}{(t_i / \zeta k_p) s^3 + (\xi t_i / \zeta k_p + t_d t_i) s^2 + t_i s + 1}. \quad (43)$$

Let $\tilde{s} = t_i s$. Then, (43) can be modified as

$$H(\tilde{s}) = \frac{\frac{t_d}{t_i} \tilde{s}^2 + \tilde{s} + 1}{\frac{1}{\zeta k_p t_i^2} \tilde{s}^3 + \left(\frac{\xi}{\zeta k_p t_i} + \frac{t_d}{t_i} \right) \tilde{s}^2 + \tilde{s} + 1} = \frac{\hat{a} \tilde{s}^2 + \tilde{s} + 1}{\hat{b} \tilde{s}^3 + (\hat{a} + \hat{c}) \tilde{s}^2 + \tilde{s} + 1} \quad (44)$$

where $\hat{a} := t_d / t_i (> 0)$, $\hat{b} := 1 / (\zeta k_p t_i^2) (> 0)$ and $\hat{c} := \xi / (\zeta k_p t_i)$. Thus, without loss of generality, the following form of the generalized frequency variable $\phi(s)$ can be considered hereafter:

$$\phi(s) = \frac{1}{\hat{H}(s)} = \frac{s}{H(s)} = \frac{\hat{b} s^4 + (\hat{a} + \hat{c}) s^3 + s^2 + s}{\hat{a} s^2 + s + 1}. \quad (45)$$

Suppose that $H(s)$ is stable so that $\hat{a} + \hat{c} > \hat{b}$. It is easily verified from (45) that $\hat{H}(s)$ does not possess non-minimum phase zeros. We define the real and the imaginary parts of $\phi(j\omega)$ in (45), $f(\omega) := \text{Re}[\phi(j\omega)]$ and $g(\omega) := \text{Im}[\phi(j\omega)]$, as follows:

$$f(\omega) = \frac{\omega^4 (-\hat{a} \hat{b} \omega^2 + \hat{b} - \hat{c})}{(1 - \hat{a} \omega^2)^2 + \omega^2}, \quad (46)$$

$$g(\omega) = \frac{(\hat{a}^2 + \hat{a} \hat{c} - \hat{b}) \omega^5 + (1 - 2\hat{a} - \hat{c}) \omega^3 + \omega}{(1 - \hat{a} \omega^2)^2 + \omega^2}. \quad (47)$$

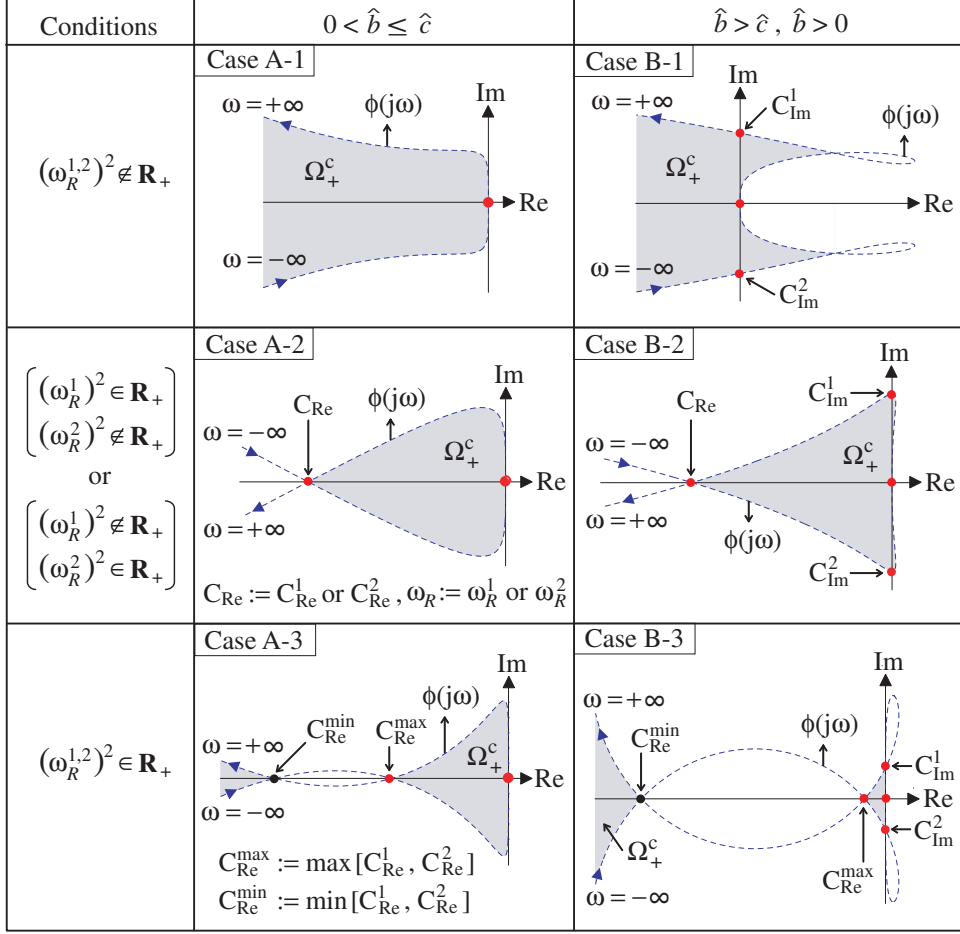


Figure 11: The image of $\phi(j\omega)$ and the domain Ω_+^c

Then, the image of $\phi(j\omega)$ yields six types of diagrams as shown in Figure 11 where \mathbf{R}_+ denotes the positive real number. If $\hat{b} > \hat{c}$ which is equivalent to $\xi < (1/t_i)$, the image of $\phi(j\omega)$ corresponds to Case A-1, A-2 or A-3; otherwise, it corresponds to Case B-1, B-2 or B-3. In this figure, C_{Im}^1 and C_{Im}^2 are determined as $C_{Im}^{1,2} = g(\omega_I^{1,2})$ where

$$\omega_I^{1,2} = \pm \left[\frac{\hat{b} - \hat{c}}{\hat{a}\hat{b}} \right]^{1/2} \in \mathbb{R}. \quad (48)$$

On the other hand, C_{Re}^1 and C_{Re}^2 are determined as $C_{Re}^{1,2} = f(\omega_R^{1,2})$ where

$$(\omega_R^{1,2})^2 = \frac{(2\hat{a} + \hat{c} - 1) \pm [\hat{c}^2 - 2(2\hat{a} - 2\hat{b} + \hat{c}) + 1]^{1/2}}{2(\hat{a}^2 + \hat{a}\hat{c} - \hat{b})} \in \mathbb{R}. \quad (49)$$

Remark 1 When the PI controller of form $K_{\text{PI}}(s) = k_p(1 + 1/(t_i s))$ is introduced, $\phi(j\omega)$ is obtained as

$$\phi_{\text{PI}}(s) = \frac{1}{\hat{H}_{\text{PI}}(s)} = \frac{s}{H_{\text{PI}}(s)} = \frac{\hat{b}s^4 + \hat{c}s^3 + s^2 + s}{s + 1} \quad (50)$$

where $\hat{c} > \hat{b} (> 0)$ which guarantees the stability of $H_{\text{PI}}(s)$. Also, from (50), we have

$$f_{\text{PI}}(\omega) := \text{Re}[\phi_{\text{PI}}(j\omega)] = \frac{\omega^4(b - c)}{\omega^2 + 1}, \quad (51)$$

$$g_{\text{PI}}(\omega) := \text{Im}[\phi_{\text{PI}}(j\omega)] = \frac{-\omega(\hat{b}\omega^4 + (\hat{c} - 1)\omega^2 - 1)}{\omega^2 + 1}. \quad (52)$$

Hence, the frequency ω_I satisfying $f_{\text{PI}}(\omega_I) = 0$ is $\omega_I = 0$. On the other hand, the frequency $\omega_R^{1,2} (\neq 0)$ satisfying $g_{\text{PI}}(\omega_R^{1,2}) = 0$ are

$$(\omega_R^{1,2})^2 = \frac{(1 - c) \pm [(1 - c)^2 + 4b]^{1/2}}{2b}. \quad (53)$$

However, since $(\omega_R^2)^2 = \{(1 - c) - [(1 - c)^2 + 4b]^{1/2}\}/2b < 0$, ω_R^2 cannot be a solution of $g_{\text{PI}}(\omega) = 0$. Note that $\omega_R^1 \in \mathbb{R}$ always exists. Therefore, the image of $\phi_{\text{PI}}(j\omega)$ corresponds to Case A-2.

5.1 Optimization-based design of path generator

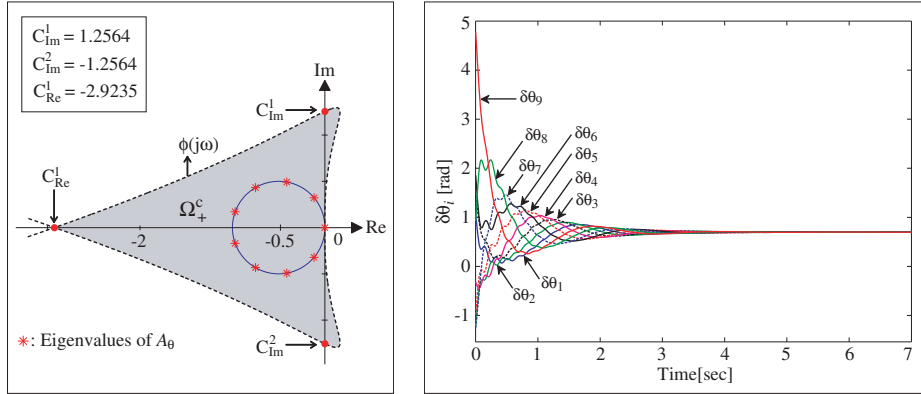
In this subsection, we examine the formation stability. As mentioned in Section 4.3, the gain k_1 in (5), which guarantees that nonzero $n - 1$ poles of $L_\theta(s)$ belong to Ω_+^c in Figure 11, can also be obtained through an optimization technique; i.e., the admissible range of k_1 is obtained by solving the following constrained optimization problem:

[Constrained optimization problem]

For $f(\omega)$ in (46) and $g(\omega)$ in (47), solve the constrained optimization problem (38) subject to $k_1 > 0$ and (39) where the range of $\omega \in \mathbb{R}$ is set as follows:

- (i) $\omega > 0$ for Case A-1,
- (ii) $0 < \omega \leq \omega_R^1$ ($\omega_R^1 > 0$) for Cases A-2 and A-3,
- (iii) $\omega \geq \omega_I^1$ for Case B-1,
- (iv) $\omega_I^1 \leq \omega \leq \omega_R^1$ ($\omega_R^1 > 0$) for Cases B-2 and B-3.

Hence, if k_1 in (5) is set as $0 < k_1 < k_{1,\text{max}}$, then all nonzero poles of $L_\theta(s)$ belong to Ω_+^c illustrated in Figure 11. Also, similarly to Theorem 4 presented in Section 4.2 the following conditions on k_2 and k_3 are easily derived from Figure 11:



(a) Domain Ω_+^c and nine eigenvalues (b) Plot showing the convergence of the angles $\delta\theta_i$ of A_θ with $k_1 = 0.5$

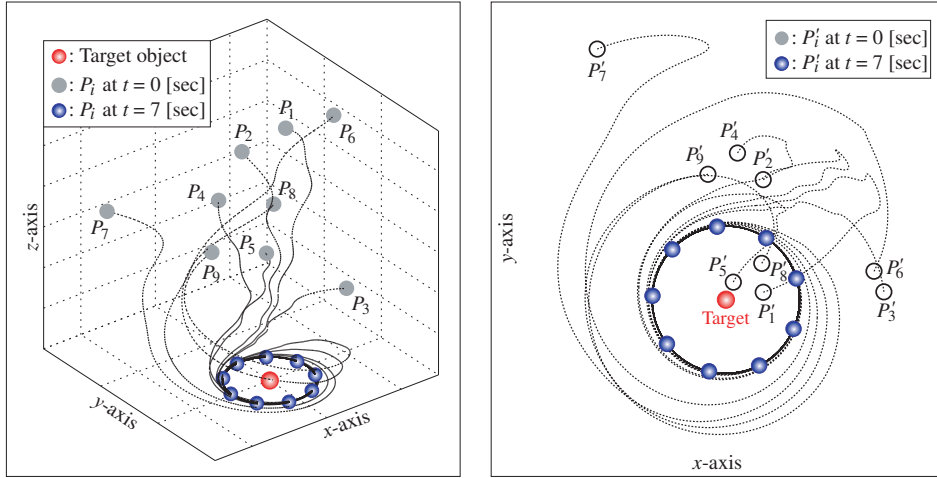
Figure 12: Plots showing the global formation stability in Example 3.

1. Cases A-1 and B-1: k_2 and k_3 can take any positive real number, since $\phi(j\omega)$ does not intersect with the real axis except at the origin.
2. Cases A-2 and B-2: $\begin{cases} C_{\text{Re}} < -k_2 < 0, \\ C_{\text{Re}} < -k_3 < 0. \end{cases}$
3. Cases A-3 and B-3: $\begin{cases} C_{\text{Re}}^{\text{max}} < -k_2 < 0 \text{ or } -k_2 < C_{\text{Re}}^{\text{min}}, \\ C_{\text{Re}}^{\text{max}} < -k_3 < 0 \text{ or } -k_3 < C_{\text{Re}}^{\text{min}}. \end{cases}$

Example 3. To illustrate the dynamic performance of the proposed distributed cooperative control scheme, a simulation is performed. Here, $n = 9$ agents are randomly dispersed in 3D space at first and finally should achieve the required formation stated in Section 2. Specifically, the desired formation is chosen to be given by $\delta\theta_i = 2\pi/9[\text{rad}]$ ($i = 1, 2, \dots, 9$), $D = 5$ and $\Phi = 0[\text{rad}]$. The initial values of $\alpha_i(t)[\text{rad}]$, $d_i(t)$ and $\theta_i(t)[\text{rad}]$ are identical to those of Example 2. Let $G(s)$ and $K(s)$ be given as

$$G(s) = \frac{1}{s(s-1)}, \quad K(s) = 12 + \frac{1}{0.2s} + 3s. \quad (54)$$

The image of $\phi(j\omega)$ corresponds to Case B-2 in Figure 11. Consequently, we set $0 < k_1 = 0.5 < k_{1,\text{max}} = 0.7856$, $0 < k_2 = 0.3 < k_{2,\text{max}} = 2.9235$ and $0 < k_3 = 0.3 < k_{3,\text{max}} = 2.9235$. Here, $k_{1,\text{max}}$ is obtained through the constrained particle swarm optimization method proposed by Maruta et al. [9, 10]. Eight nonzero eigenvalues of A_θ belong to the domain Ω_+^c , which is confirmed in Figure 12(a). The simulation results are shown in Figures 12(b) and 13. First, Figure 13(a) illustrates the resulting position trajectories of a group of nine agents during the simulation: the agents



(a) Position trajectories of all agents P_i (b) Planar trajectories of agents P_i converging to the desired formation

Figure 13: Simulation results of Example 3.

assemble into the desired configuration. Figure 13(b) depicts the trajectories of all agents projected onto x - y plane. They show that all agents converge to a circular formation around the target object and maintain the form of an equilateral and equiangular polygon. The changes of $\delta\theta_i$ with respect to time are plotted in Figure 12(b), where $\delta\theta_i$ finally converges to $2\pi/9$ [rad]. It clearly demonstrates that the control goals (A1')-(A3') mentioned in Section 3 are achieved. ■

6 Formation stability analysis based on the generalized KYP lemma

In this subsection, we show that the frequency-domain inequality (FDI) condition (28), which should be guaranteed for $\forall\omega \in \mathbb{R}\setminus\{0\}$, can be easily checked via the generalized Kalman-Yakubovich-Popov (GKYP) lemma [3, 4].

First, note that it is equivalent to (28) that

$$\begin{bmatrix} \hat{H}(j\omega) \\ 1 \end{bmatrix}^* \Pi \begin{bmatrix} \hat{H}(j\omega) \\ 1 \end{bmatrix} < 0, \quad \Pi := \begin{bmatrix} 0 & -k_1 \\ -k_1 & -1 \end{bmatrix} \quad (55)$$

for $\forall\omega \in \mathbb{R}\setminus\{0\}$. In (55), $\hat{H}(s)$ is proper as shown in (22) for PD controller case or (45) for PID controller case, and thus has the following state-space realization:

$$\hat{H}(s) = C_h(sI - A_h)^{-1}B_h + D_h. \quad (56)$$

It also should be noted that if the FDI specification in (55) is satisfied only in a specified frequency range presented in Figure 14 for PD controller case and Figure 15 for PID controller case, then the θ -directional pursuit formation stability is guaranteed. It means that one does not need to check (55) for the entire frequency range. In Figures 14 and 15, ω_ϵ and ω_∞ denote, respectively, infinitesimally small positive real number and sufficiently large positive real numbers (these are design variables), \mathbf{R}_+ denotes the positive real number, and ω_R^{\max} and ω_R^{\min} denote, respectively, the frequencies corresponding to C_{Re}^{\max} and C_{Re}^{\min} .

For the above problem, the FDI specification (55) can easily be checked by using the GKYP lemma [3, 4], which transforms a FDI in a finite (or semi-infinite) frequency range into a set of linear matrix inequalities (LMIs). In the following, a unified form of the GKYP lemma is presented.

Theorem 5 (Generalized KYP lemma [3]) *Let $\Pi \in \mathbf{H}_p$, $\Gamma, \Psi \in \mathbf{H}_2$, and define the rational function*

$$G(\lambda) := C(\lambda E - A)^{-1}(B - \lambda F) + D, \quad (57)$$

where $\lambda \in \mathbb{C}$, $A, E \in \mathbb{C}^{n \times n}$, $B, F \in \mathbb{C}^{n \times m}$, $C \in \mathbb{C}^{p \times n}$, and $D \in \mathbb{C}^{p \times m}$. Suppose i) $\det(\lambda E - A) \neq 0$ for all $\lambda \in \Lambda(\Gamma, \Psi)$ where

$$\Lambda(\Gamma, \Psi) := \left\{ \lambda \in \mathbb{C} : \begin{bmatrix} \lambda \\ 1 \end{bmatrix}^* \Gamma \begin{bmatrix} \lambda \\ 1 \end{bmatrix} = 0, \begin{bmatrix} \lambda \\ 1 \end{bmatrix}^* \Psi \begin{bmatrix} \lambda \\ 1 \end{bmatrix} \geq 0 \right\}, \quad (58)$$

and ii) either E is nonsingular or Λ is bounded. Then, the parameterized inequality condition

$$G(\lambda)^* \Pi G(\lambda) < 0, \text{ for all } \lambda \in \bar{\Lambda}(\Gamma, \Psi) \quad (59)$$

where $\bar{\Lambda}$ is defined as

$$\bar{\Lambda} := \begin{cases} \Lambda & \text{if } \Lambda \text{ is bounded} \\ \Lambda \cup \{\infty\} & \text{otherwise} \end{cases} \quad (60)$$

holds if and only if there exist matrices $P, Q \in \mathbf{H}_n$ satisfying

$$Q > 0, \quad M^* Z M < 0, \quad Z = \text{diag}(\Gamma \otimes P + \Psi \otimes Q, \Pi) \quad (61)$$

where H is defined by

$$M := \begin{bmatrix} A & B \\ E & F \\ C & D \end{bmatrix}. \quad (62)$$

The above presented GKYP lemma means that checking the FDI in (55) within a given frequency range specified in Figures 14 and 15 can be converted to the search for matrices $P, Q \in \mathbf{H}_n$ satisfying the LMI in (61).

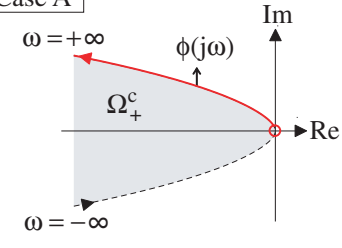
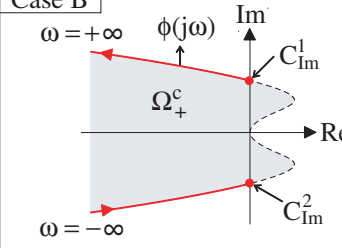
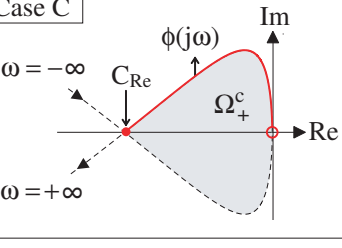
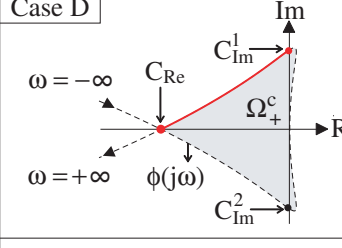
Conditions	$b > 1$	$0 < b \leq 1$
$0 < a < b$	<div style="border: 1px solid black; padding: 5px;"> Case A  </div>	<div style="border: 1px solid black; padding: 5px;"> Case B  </div>
	Frequency range: $\omega_\varepsilon \leq \omega \leq \omega_\infty$ $\Psi = \begin{bmatrix} -1 & j\omega_o \\ -j\omega_o & -\omega_\varepsilon \omega_\infty \end{bmatrix}$ $\omega_o := (\omega_\varepsilon + \omega_\infty) / 2$	Frequency range: $ \omega \geq \omega_l^1$ $\Psi = \begin{bmatrix} 1 & 0 \\ 0 & -(\omega_l^1)^2 \end{bmatrix}$
$a \geq b > 0$	<div style="border: 1px solid black; padding: 5px;"> Case C  </div>	<div style="border: 1px solid black; padding: 5px;"> Case D  </div>
	Frequency range: $\omega_\varepsilon \leq \omega \leq \omega_R$ $\Psi = \begin{bmatrix} -1 & j\omega_o \\ -j\omega_o & -\omega_\varepsilon \omega_R \end{bmatrix}, \omega_R > 0$ $\omega_o := (\omega_\varepsilon + \omega_R) / 2$	Frequency range: $\omega_l^1 \leq \omega \leq \omega_R$ $\Psi = \begin{bmatrix} -1 & j\omega_o \\ -j\omega_o & -\omega_l^1 \omega_R \end{bmatrix}, \omega_R > 0$ $\omega_o := (\omega_l^1 + \omega_R) / 2$

Figure 14: PD controller case: Four types of ranges of ω and the corresponding Ψ

Note that LMIs are numerically tractable and can be solved efficiently. In our problem setting, $\Psi \in \mathbf{H}_2$ is set as defined in Figure 14 for PD controller case and Figure 15 for PID controller case. On the other hand, $\Gamma \in \mathbf{H}_2$ is set as

$$\Gamma := \begin{bmatrix} 0 & 1 \\ 1 & 0 \end{bmatrix}, \quad (63)$$

since the continuous-time setting is considered in this paper. For details of choices of Γ and Ψ , refer to Iwasaki and Hara [4].

The following example illustrates how to examine the formation stability via the GKYP lemma.

Example 4. The image $\phi(j\omega)$ of (22) with $G_\theta(s) = 1/s(s-2)$ and $K_\theta(s) =$

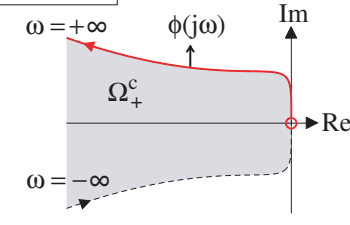
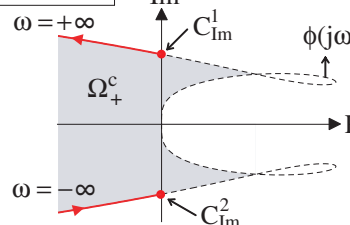
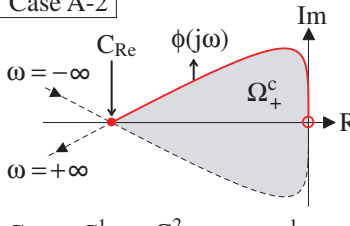
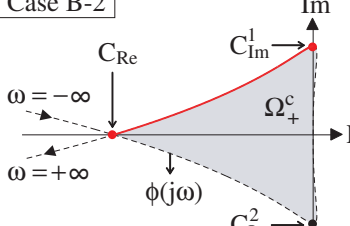
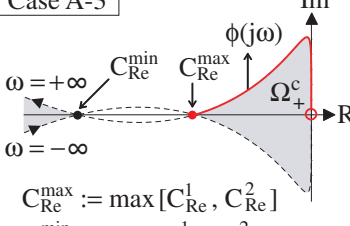
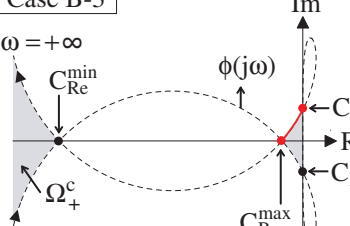
Conditions	$0 < \hat{b} \leq \hat{c}$	$\hat{b} > \hat{c}, \hat{b} > 0$
$(\omega_R^{1,2})^2 \notin \mathbf{R}_+$	Case A-1 	Case B-1 
	Frequency range: $\omega_\varepsilon \leq \omega \leq \omega_\infty$ $\Psi = \begin{bmatrix} -1 & j\omega_o \\ -j\omega_o & -\omega_\varepsilon \omega_\infty \end{bmatrix}$ $\omega_o := (\omega_\varepsilon + \omega_\infty)/2$	Frequency range: $ \omega \geq \omega_I^1$ $\Psi = \begin{bmatrix} 1 & 0 \\ 0 & -(\omega_I^1)^2 \end{bmatrix}$
$(\omega_R^1)^2 \in \mathbf{R}_+$ $(\omega_R^2)^2 \notin \mathbf{R}_+$ or $(\omega_R^1)^2 \notin \mathbf{R}_+$ $(\omega_R^2)^2 \in \mathbf{R}_+$	Case A-2 	Case B-2 
	Frequency range: $\omega_\varepsilon \leq \omega \leq \omega_R$ $\Psi = \begin{bmatrix} -1 & j\omega_o \\ -j\omega_o & -\omega_\varepsilon \omega_R \end{bmatrix}, \omega_R > 0$ $\omega_o := (\omega_\varepsilon + \omega_R)/2$	Frequency range: $\omega_I^1 \leq \omega \leq \omega_R$ $\Psi = \begin{bmatrix} -1 & j\omega_o \\ -j\omega_o & -\omega_I^1 \omega_R \end{bmatrix}, \omega_R > 0$ $\omega_o := (\omega_I^1 + \omega_R)/2$
$(\omega_R^{1,2})^2 \in \mathbf{R}_+$	Case A-3 	Case B-3 
	Frequency range: $\omega_\varepsilon \leq \omega \leq \omega_R^{\max}$ $\Psi = \begin{bmatrix} -1 & j\omega_o \\ -j\omega_o & -\omega_\varepsilon \omega_R^{\max} \end{bmatrix}, \omega_R^{\max} > 0$ $\omega_o := (\omega_\varepsilon + \omega_R^{\max})/2$	Frequency range: $\omega_I^1 < \omega < \omega_R^{\max}$ $\Psi = \begin{bmatrix} -1 & j\omega_o \\ -j\omega_o & -\omega_I^1 \omega_R^{\max} \end{bmatrix}, \omega_R^{\max} > 0$ $\omega_o := (\omega_I^1 + \omega_R^{\max})/2$

Figure 15: PID controller case: Six types of ranges of ω and the corresponding Ψ

$1 + 4s$ corresponds to the Case B in Figure 14 ($a = 0.0625$, $b = 0.5$). In this case, the frequency range to be considered is $|\omega| \geq \omega_I^1 \approx 0.7071$, and thus Ψ is set as $\Psi = \begin{bmatrix} 1 & 0 \\ 0 & -0.7071^2 \end{bmatrix}$. Consider the case $k_1 = 0.7$, which leads to $\Pi = \begin{bmatrix} 0 & -0.7 \\ -0.7 & -1 \end{bmatrix}$. Then, the matrices $P, Q \in \mathbf{H}_3$ satisfying (61) are obtained as

$$P = \begin{bmatrix} 1.9831 & 1.9649 & 0.6998 \\ 1.9649 & 6.8831 & 1.4271 \\ 0.6998 & 1.4271 & 0.6996 \end{bmatrix}, \quad Q = \begin{bmatrix} 0.6082 & 0 & 1.1599 \\ 0 & 0.0723 & 0 \\ 1.1599 & 0 & 2.4494 \end{bmatrix}$$

via the LMI Control Toolbox in MATLAB. It means that all nonzero eigenvalues of A_θ are placed in the domain Ω_+^c , and thus the formation stability is guaranteed. On the other hand, if $k_1 = 0.8$, no feasible $P, Q \in \mathbf{H}_3$ are found, which means the formation instability. ■

Remark 2 *Some of the coefficients in Ψ defined in Figures 14 and 15 are complex and, therefore, the variables P and Q must be sought over the set of complex matrices. However, some LMI solvers, such as the LMI Control Toolbox in MATLAB, can handle LMIs with real coefficients and real variables only. To overcome this limitation, a complex LMI can be converted to a real LMI of larger dimension through the equivalence of $X + jY = (X + jY)^*$ and*

$$\begin{bmatrix} X & Y \\ -Y & X \end{bmatrix} = \begin{bmatrix} X & Y \\ -Y & X \end{bmatrix}^T > 0,$$

where X and Y are real square matrices representing the real and imaginary parts of the complex LMI [3].

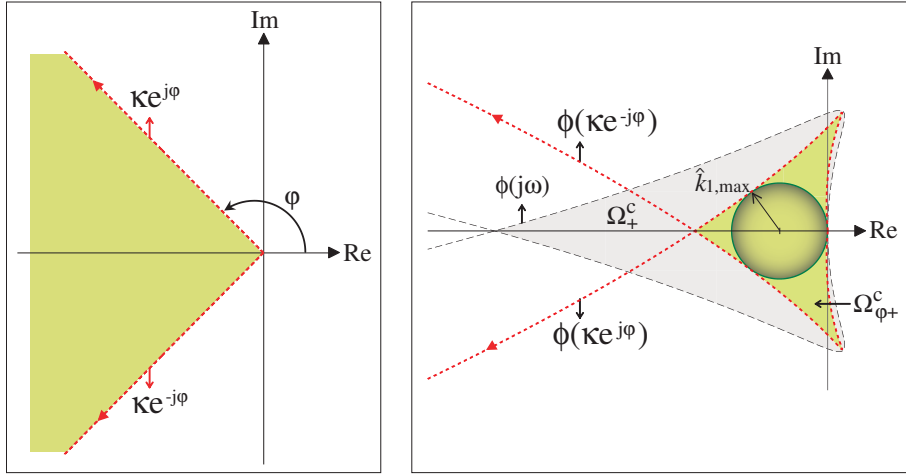
7 Pole assignment scheme for target-enclosing formation control

In this section, we consider the following problem: how to set k_1 in (5) so that all the poles of $\mathcal{G}_\theta(s) (= L_\theta(\phi(s)))$ in (14) are placed in a predesignated region; e.g., the shaded region in Figure 16(a) where $\kappa \geq 0$ and φ satisfying $0 \leq \varphi \leq \pi$ is given a priori.

First, similar to the definition of domains Ω_+ and Ω_+^c in (17), the domains $\Omega_{\varphi+}$ and $\Omega_{\varphi+}^c$ in the complex plane are defined as follows:

$$\Omega_{\varphi+} := \phi(\mathbb{C}_{\varphi+}), \quad \Omega_{\varphi+}^c := \mathbb{C} \setminus \Omega_{\varphi+}, \quad (64)$$

where $\mathbb{C}_{\varphi+} = \{s := \kappa e^{j\vartheta} \in \mathbb{C} : -\varphi \leq \vartheta \leq \varphi, \forall \kappa > 0\}$. Note that the domain $\Omega_{\varphi+}^c$ includes the origin of the complex plane. Hence, we can see that if all the eigenvalues (27) of A_θ belong to the domain $\Omega_{\varphi+}^c$ characterized by $\kappa e^{\pm j\varphi}$, then all the poles of $\mathcal{G}_\theta(s)$ are located in the predesignated region.



(a) The predesignated region for locations of all the poles of $\mathcal{G}_\theta(s)$ (b) The domain $\Omega_{\phi+}^c$ and the image of $\phi(\kappa e^{\pm j\varphi})$ where $\kappa \geq 0$ and $0 \leq \varphi \leq \pi$

Figure 16: The image of $\phi(\kappa e^{\pm j\varphi})$ and the corresponding domain $\Omega_{\phi+}^c$

In this case, the maximum value of k_1 in (5), which guarantees the above-mentioned property, can be readily obtained by solving the following constrained optimization problem:

[Constrained optimization problem]

For $f_\varphi(\kappa)$ and $g_\varphi(\kappa)$ defined, respectively, as

$$f_\varphi(\kappa) := \text{Re}[\phi(\kappa e^{j\varphi})], \quad g_\varphi(\kappa) := \text{Im}[\phi(\kappa e^{j\varphi})] \quad (65)$$

where φ is given a priori, solve

$$\hat{k}_{1,\max} := \arg \max_{k_1, \kappa} k_1 \quad (66)$$

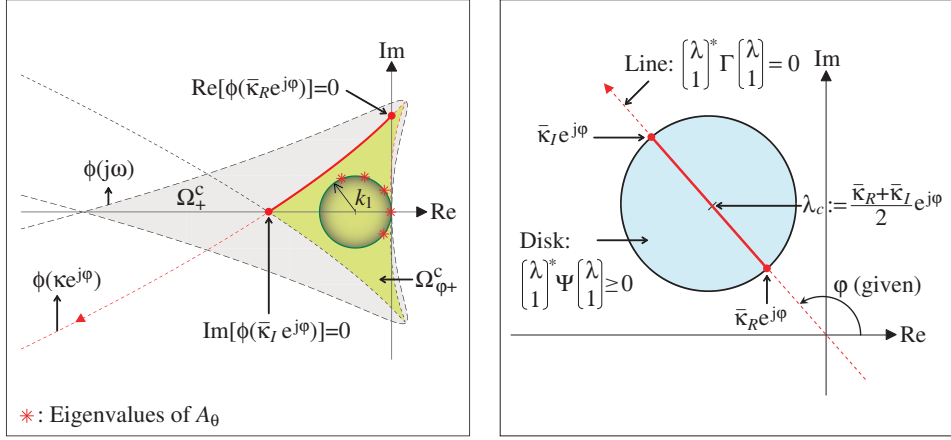
subject to

$$(f_\varphi(\kappa) + \hat{k}_1)^2 + g_\varphi^2(\kappa) \geq \hat{k}_1^2, \quad \hat{k}_1 > 0, \quad \kappa > 0. \quad (67)$$

Therefore, if one sets k_1 in (5) as $0 < k_1 < \hat{k}_{1,\max}$, then all the poles of $\mathcal{G}_\theta(s)$ in (14) are placed in the predesignated region. It is a considerably simple pole assignment technique. This fact is verified through the numerical example presented at the end of this subsection.

On the other hand, it can be easily checked based on the GKYP lemma whether all the eigenvalues of A_θ with k_1 given a priori exist inside the domain Ω_+^c or not; i.e., the following inequality condition needs to be checked:

$$\begin{bmatrix} \hat{H}(\kappa e^{j\varphi}) \\ 1 \end{bmatrix}^* \Pi \begin{bmatrix} \hat{H}(\kappa e^{j\varphi}) \\ 1 \end{bmatrix} < 0, \quad \Pi := \begin{bmatrix} 0 & -k_1 \\ -k_1 & -1 \end{bmatrix}, \quad \forall \kappa > 0, \quad (68)$$



(a) The image of $\phi(\kappa e^{\pm j\varphi})$, $\forall \kappa \geq 0$, where φ (rad) is given. (b) The set of complex numbers determined by $\Lambda(\Gamma, \Psi)$ where Γ, Ψ are set as

Figure 17: The image of $\phi(\kappa e^{j\varphi})$ and the set of complex numbers $\Lambda(\Gamma, \Psi)$

for given k_1 and φ . In order to check (68) within a framework of GKYP lemma, we first characterize the range of κ . For example, in case that $\phi(s) (= 1/\hat{H}(s))$ and φ are given, $\phi(\kappa e^{j\varphi})$ is readily obtained (see Figure 17). Then, $\bar{\kappa}_R$ and $\bar{\kappa}_I$ ($0 < \bar{\kappa}_R < \bar{\kappa}_I$) satisfying $\text{Re}[\phi(\bar{\kappa}_R e^{j\varphi})] = 0$ and $\text{Im}[\phi(\bar{\kappa}_I e^{j\varphi})] = 0$ respectively are found via simple calculations (if exist). Now one can see from Figure 17(a) that it is sufficient to check the condition (68) in the range $\bar{\kappa}_R \leq \kappa \leq \bar{\kappa}_I$. In this case, the set of complex numbers $\Lambda(\Gamma, \Psi)$ corresponding to the above-mentioned range of κ is defined as

$$\Lambda(\Gamma, \Psi) := \left\{ \lambda \in \mathbb{C} : \begin{bmatrix} \lambda \\ 1 \end{bmatrix}^* \Gamma \begin{bmatrix} \lambda \\ 1 \end{bmatrix} = 0, \begin{bmatrix} \lambda \\ 1 \end{bmatrix}^* \Psi \begin{bmatrix} \lambda \\ 1 \end{bmatrix} \geq 0 \right\}, \quad (69)$$

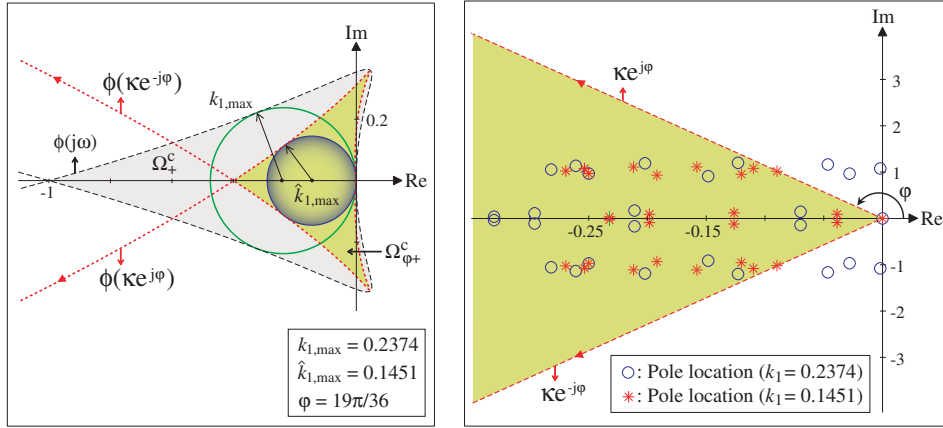
where

$$\Gamma := \begin{bmatrix} 0 & \tan \varphi - j \\ \tan \varphi + j & 0 \end{bmatrix}, \quad \Psi := \begin{bmatrix} -1 & \lambda_c \\ \bar{\lambda}_c & -\bar{\kappa}_R \bar{\kappa}_I \end{bmatrix}, \quad (70)$$

and $\lambda_c = \frac{\bar{\kappa}_R + \bar{\kappa}_I}{2} e^{j\varphi}$ (see Figure 17(b)). Hence, under the above setting (69)-(70), the formation stability condition of form (68) can easily be confirmed through the GKYP lemma presented in Section 6. Its effectiveness is illustrated in the following numerical example.

Remark 3 A set of complex numbers $\Lambda(\Gamma, \Psi)$ is the intersection of $\Lambda(\Gamma, 0)$ and $\Lambda(0, \Psi)$, and represents a certain class of curves. Note that the type of curves depends on the choices of Γ and Ψ . For example, a circle of radius r_c with center at λ_c is represented as

$$\begin{bmatrix} \lambda \\ 1 \end{bmatrix}^* \begin{bmatrix} 1 & -\lambda_c \\ -\bar{\lambda}_c & |\lambda_c|^2 - r_c^2 \end{bmatrix} \begin{bmatrix} \lambda \\ 1 \end{bmatrix} = |\lambda - \lambda_c|^2 - r_c^2 = 0, \quad (71)$$



(a) The images of $\phi(j\omega)$, $\phi(\kappa e^{j\varphi})$ and the corresponding domains Ω_+^c , $\Omega_{\varphi+}^c$ (b) The pole locations of $\mathcal{G}_\theta(s)$ with two different values of k_1

Figure 18: Simulation results of numerical example in Section 7.1

and a straight line with the normal vector $a + jb \neq 0$ is represented as

$$\begin{bmatrix} \lambda \\ 1 \end{bmatrix}^* \begin{bmatrix} 0 & a + jb \\ a - jb & 2c \end{bmatrix} \begin{bmatrix} \lambda \\ 1 \end{bmatrix} = 2(a\text{Re}[\lambda] + b\text{Im}[\lambda] + c) = 0. \quad (72)$$

The matrices Γ and Ψ given in (70) are derived from (71)-(72). For details, refer to [3, 4].

7.1 Numerical example

Suppose that $n = 9$ agents have common dynamics $G_\theta(s) = 1/(s(s - 0.5))$ and its stabilizing PD controller is given as $K_\theta(s) = 1 + s$. In this case, the images of $\phi(j\omega)$ and $\phi(\kappa e^{j\varphi})$ with $\varphi = 19\pi/36$ (rad) are illustrated in Figure 18(a). Here, $k_{1,\max} = 0.2374$ and $\hat{k}_{1,\max} \approx 0.1451$ are obtained by solving the constrained optimization problems given respectively in Sections 4.3 and 7 through the constrained particle swarm optimization scheme [9, 10]. Then, all pole locations of $\mathcal{G}_\theta(s)$ with $k_1 = 0.2374$ or $k_1 = 0.1451$ are depicted in Figure 18(b). From this figure, it can be easily confirmed that if it is required for all the poles of $\mathcal{G}_\theta(s)$ in (14) to be assigned to a predesignated region (the shaded region in Figure 18(b)), the only thing one should do is to find $\hat{k}_{1,\max}$ and then set k_1 as $0 \leq k_1 \leq \hat{k}_{1,\max}$. The above fact shows that it is an easily implementable pole assignment technique. The time plots of $\delta\theta_i(t)$ ($i = 1, 2, \dots, 8$) for $k = 0.1451$ and 0.2374 are illustrated in Figure 19.

Next, we show that the specification (68) with a given k_1 can readily be examined through the GKYP lemma under (69)-(70). From the above-mentioned multiple agent system with $k_1 = 0.12$ and $\varphi = 19\pi/36$, we obtain

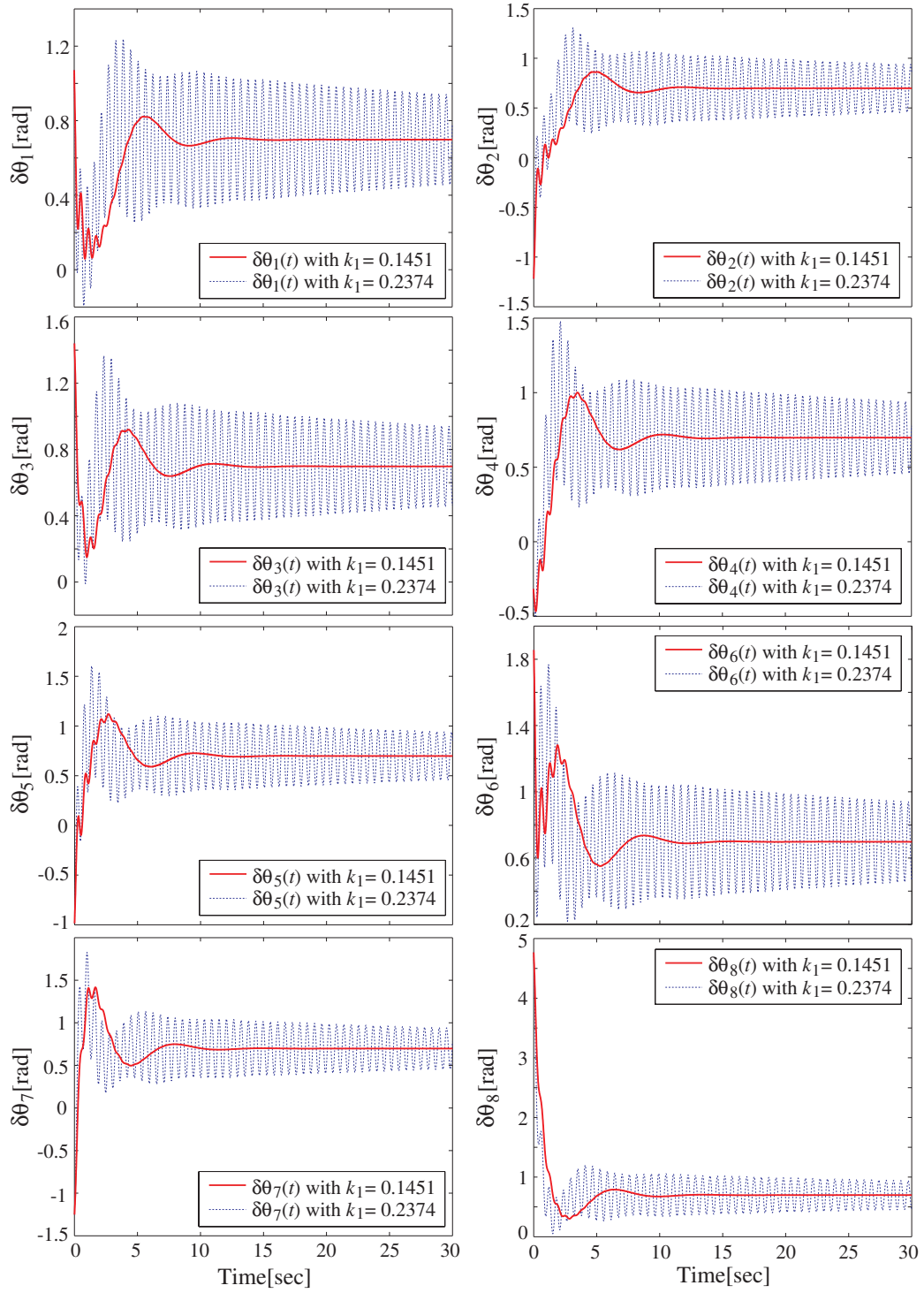


Figure 19: Time plots of $\delta\theta_i$ ($i = 1, 2, \dots, 8$) for $k_1 = 0.1451$ and 0.2374

$\bar{\kappa}_R \approx 0.7490$ and $\bar{\kappa}_I \approx 1.1573$. Then, by using the LMI Control Toolbox in MATLAB, the matrices $P, Q \in \mathbf{H}_3$ satisfying the LMI in (61) with Γ and Ψ in (68)-(70) are obtained as

$$P = 10^3 \times \begin{bmatrix} 0.5821 & 0.1969 - 1.1302j & -0.5316 - 0.1822j \\ 0.1969 + 1.1302j & 2.2809 & 0.1795 - 1.1170j \\ -0.5316 + 0.1822j & 0.1795 + 1.1170j & 0.5690 \end{bmatrix},$$

$$Q = \begin{bmatrix} 11.1358 & 5.3084 - 21.4341j & -9.5893 - 5.0699j \\ 5.3084 + 21.4341j & 43.9731 & 5.2354 - 21.0703j \\ -9.5893 + 5.0699j & 5.2354 + 21.0703j & 10.7849 \end{bmatrix}.$$

It means that all the eigenvalues of A_θ exist in the domain $\Omega_{\varphi_+}^c$. Note that Γ and Ψ of this example are complex-valued matrices. Thus, we introduced the procedure presented in Remark 2 to turn complex-valued LMIs into real-valued LMIs. ■

8 Conclusion

In this paper, we presented a design methodology of a distributed cooperative controller for target-enclosing operations by multiple dynamic agents. To this end, we first presented an on-line path generator design method based on a cyclic pursuit scheme. Then, we provided the stability condition which the developed path generator should satisfy. This condition was derived based on a considerably simple unified stability analysis method for hierarchical large-scale linear systems with a generalized frequency variable. The formation control scheme combined with a cyclic pursuit based distributed on-line path generator satisfying the derived stability condition guarantees the required global formation stability with theoretical rigor. Further, in order to show clearly its distinctive features, we presented how to develop a cyclic pursuit based formation control strategy for a class of multi-agent systems where each agent is modeled as a second-order system and is locally stabilized by the PD/PID controllers. It was also presented that the formation stability analysis can be easily performed based on the generalized Kalman-Yakubovich-Popov (KYP) lemma. Its effectiveness was verified through simulation examples.

References

- [1] J. A. Fax and R. M. Murray. Information flow and cooperative control of vehicle formations. *IEEE Transactions on Automatic Control*, 49(9):1465–1476, 2004.
- [2] S. Hara, T. Hayakawa, and H. Sugata. Stability analysis of linear systems with generalized frequency variables and its application to forma-

- tion control. In *Proceedings of the 46th IEEE Conference on Decision and Control*, pages 1459–1466, New Orleans, LA, USA, 2007.
- [3] S. Hara, T. Iwasaki, and D. Shiokata. Robust PID control using generalized KYP synthesis: direct open-loop shaping in multiple frequency ranges. *IEEE Control Systems Magazine*, 26(1):80–91, 2006.
 - [4] T. Iwasaki and S. Hara. Generalized KYP lemma: Unified frequency domain inequalities with design applications. *IEEE Transactions on Automatic Control*, 50(1):41–59, 2004.
 - [5] T.-H. Kim and T. Sugie. Cooperative control for target-capturing task based on a cyclic pursuit strategy. *Automatica*, 43(8):1426–1431, 2007.
 - [6] K. Kobayashi, K. Otsubo, and S. Hosoe. Design of decentralized capturing behavior by multiple robots. In *IEEE Workshop on Distributed Intelligent Systems: Collective Intelligence and its applications*, pages 463–468, 2006.
 - [7] J. A. Marshall, M. E. Broucke, and B. A. Francis. Formations of vehicles in cyclic pursuit. *IEEE Transactions on Automatic Control*, 49(11):1963–1974, 2004.
 - [8] J. A. Marshall, M. E. Broucke, and B. A. Francis. Pursuit formations of unicycles. *Automatica*, 42:3–12, 2006.
 - [9] I. Maruta, T.-H. Kim, and T. Sugie. New constrained particle swarm optimization and its application to controller design with fixed structure. In *The 36th SICE Symposium on Control Theory*, pages 255–260, 2007.
 - [10] I. Maruta, T.-H. Kim, and T. Sugie. Synthesis of fixed-structure H_∞ controllers via constrained particle swarm optimization. In *Proceedings of the 17th IFAC World Congress*, Seoul, Korea, 2008. (to appear).
 - [11] R. Olfati-Saber, J. A. Fax, and R. M. Murray. Consensus and cooperation in networked multi-agent systems. *Proceedings of the IEEE*, 95(1):215–233, 2007.
 - [12] R. Sepulchre, D. A. Paley, and N. E. Leonard. Group coordination and cooperative control of steered particles in the plane. In *Group Coordination and Cooperative Control*, pages 217–232. Springer-Verlag: Lecture Notes in Control and Information Sciences, 2006.
 - [13] A. Sinha and D. Ghose. Generalization of linear cyclic pursuit with application to rendezvous of multiple autonomous agents. *IEEE Transactions on Automatic Control*, 51(11):1819–1824, 2006.